

# Yano-Koonin-Podgoretskiĭ Parametrisation of the Hanbury Brown-Twiss Correlator

Wu Y.-F.<sup>1,\*</sup>, U. Heinz<sup>1,2</sup>, B. Tomášik<sup>1</sup>, and U.A. Wiedemann<sup>1</sup>

<sup>1</sup>*Institut für Theoretische Physik, Universität Regensburg,*

*D-93040 Regensburg, Germany*

<sup>2</sup>*CERN/TH, CH-1211 Geneva 23, Switzerland*

(June 11, 1997)

## Abstract

The Yano-Koonin-Podgoretskiĭ (YKP) parametrisation of Hanbury Brown-Twiss (HBT) two-particle correlation functions opens new strategies for extracting the emission duration and testing the longitudinal expansion in heavy-ion collisions. Based on the recently derived model-independent expressions, we present a detailed parameter study of the YKP parameters for a finite, hydrodynamically expanding source model of heavy-ion collisions. For the class of models studied here, we show that the three YKP radius parameters have an interpretation as longitudinal extension, transverse extension and emission duration of the source in the YKP frame. This frame is specified by the fourth fit parameter, the Yano-Koonin velocity which describes to a good approximation the velocity of the fluid element with highest emissivity and allows to test for the longitudinal expansion of the source. Deviations from this interpretation of the YKP parameters are discussed quantitatively.

PACS numbers: 25.75.Gz, 25.75.Ld, 12.38.Mh

## I. INTRODUCTION

The spatio-temporal extension and evolution of the interaction region in heavy-ion collisions are not directly observable. Indirect experimental access to its geometry and dynamics is possible through Hanbury Brown-Twiss (HBT) intensity interferometry [1,2]. However, the interpretation of the measured HBT correlations is in general model dependent, and the question arises to what extent their interpretational ambiguity can be reduced by a refined analysis of the data.

In general, HBT radius parameters measure the Gaussian widths (second central moments) of the source distribution in space-time [3–7]. It is the finite lifetime of the particle source in heavy ion collisions which complicates their interpretation. For a static boson emitting source, the HBT-radii have a *unique* interpretation in terms of geometrical source sizes. For dynamical sources like those created in heavy ion collisions, however, the HBT-radii measure certain linear combinations of the lifetime, the geometrical sizes and other space-time correlations [3–5,7,8]. Furthermore, if the source expands all HBT parameters become functions of the pair momentum [9,6].

For azimuthally symmetric sources, corresponding to heavy-ion collisions at zero impact parameter, there exist two different “complete” Gaussian parametrizations for the correlation function: the Cartesian parametrization with parameters  $R_s$ ,  $R_o$ ,  $R_l$  and  $R_{ol}$  [8,9,3,4], and the Yano-Koonin-Podgoretskiĭ (YKP) parametrisation with parameters  $R_\perp$ ,  $R_\parallel$ ,  $R_0$  and  $v$  [10–12,5,7]. In each case, for expanding sources, these parameters are functions of the pair momentum. The  $R$ -parameters have the dimension of a length while  $v$  is a velocity. The Cartesian parametrization has the additional difficulty that the value and the spatio-temporal interpretation of its parameters depend strongly on the longitudinal rest frame of the observer. The YKP radius parameters  $R_\perp$ ,  $R_\parallel$ , and  $R_0$ , on the other hand, are independent of the longitudinal velocity of the frame in which the particle momenta are measured. The fourth YKP fit parameter, the Yano-Koonin velocity  $v$ , singles out a specific longitudinal rest frame (relative to the observer) in which the spatio-temporal interpretation

of the (longitudinally boost-invariant) YKP-radius parameters becomes particularly simple. In fact, for “transparent” sources (i.e. sources, for which particle emission occurs from the whole volume and is not surface dominated) without collective transverse expansion, it was shown in [5] that  $R_\perp$ ,  $R_\parallel$ , and  $R_0$  give exactly the transverse, longitudinal and temporal widths respectively, of the source emission function in the Yano-Koonin frame where  $v = 0$ . We will show here that in this case, up to small corrections from asymmetries of the source rapidity profile due to longitudinal expansion flow,  $v$  coincides with the longitudinal velocity of the fluid element around the point of highest emissivity in the source, such that  $R_\perp$ ,  $R_\parallel$  and  $R_0$  measure (and cleanly separate) the transverse, longitudinal and temporal lengths of homogeneity of the source in the rest frame of the emitter. As discussed in Sec. IV A, the pair momentum dependence of  $v$  allows to measure the longitudinal expansion of the source in a very direct way.

For the class of models studied here, we will also show (see Sec. IV D) that in the absence of transverse collective expansion the YKP parameters show perfect  $M_\perp$ -scaling, i.e., they are, for a given source, universal functions of the transverse mass  $M_\perp = \sqrt{m^2 + \mathbf{K}_\perp^2}$  of the particle pair, independent of the particle rest mass. This can be tested by comparing  $\pi\pi$ ,  $KK$ , and  $pp$  correlations. The same is not true for the Cartesian parameters which contain additional kinematic and frame dependent factors which distinguish between pairs of particles with different mass. This type of  $M_\perp$  scaling of the YKP parameters is violated for sources with transverse collective expansion; also other types of transverse  $x$ - $p$ -correlations, like e.g. those occurring in opaque sources [13], and final state effects like resonance decays after freeze-out [14], can break this scaling. For a detailed discussion of these effects see Refs. [15] (opaque sources) and [16,17] (resonance decays).

One of the purposes of this paper is to investigate the specific effects on the correlator and the related corrections to the spatio-temporal interpretation of the YKP parameters introduced by transverse expansion flow in the source. These will in general depend on the particular source model, and such an investigation thus must necessarily involve an extensive model study. We investigate here numerically a simple parametrization of the source which

implements the finite longitudinal, transverse and temporal extension and the longitudinal expansion of realistic heavy-ion generated sources and contains the transverse expansion flow as a tunable parameter. We will see that strong transverse flow affects the interpretation of the YKP parameter  $R_0$  as the lifetime of the source (in its own rest frame) and thus renders the extraction of the duration of particle emission from the correlation data more difficult and less quantitatively reliable. On the other hand, it also spoils the  $M_\perp$ -scaling of the YKP radius parameters which opens the possibility for an independent estimate of the transverse flow velocity from comparison between pion and kaon correlations. Clearly, such an estimate will remain somewhat model-dependent, but the mechanisms isolated in the present paper should still be very useful for qualitative consistency checks between data and theoretical interpretation.

The investigation reported here has two aspects: an analytical and a numerical one. On the analytical level, we study the connection between the YKP parameters and the second space-time moments of the emission function, discussing the dependence of the latter on various geometric and dynamical features of particle emission. This discussion is largely model-independent; it is much more detailed than the short account given in [7] and should thus serve as a general basis of understanding which can be used to qualitatively anticipate the behaviour of the YKP parameters also for other source models than the one studied here. The numerical side of our study is, of course, model-dependent and our quantitative results must therefore be regarded with the necessary caution.

Our paper is organized as follows: In Sec. II, we shortly compare the Cartesian and YKP parametrizations, thereby setting up our notation. In Sec. III, we introduce a class of hydrodynamical models for the emission function. Sec. IV contains a general discussion and a detailed numerical study of these models. We focus in particular on the effects of collective expansion flow on the YKP parameters. The main results are summarized in Sec. V.

## II. HBT FORMALISM

We shortly recall the basic relations between the emission function  $S(x, K)$ , the measured two-particle correlation function  $C(\mathbf{q}, \mathbf{K})$ , and the different Gaussian parametrisations of this correlator in terms of Cartesian or YKP radius parameters. We start from the relation [18,1,9,19] (here written down for bosons)

$$C(\mathbf{q}, \mathbf{K}) \approx 1 + \frac{|\int d^4x S(x, K) e^{iq \cdot x}|^2}{|\int d^4x S(x, K)|^2}. \quad (2.1)$$

Here, the emission function  $S(x, p)$  is the (Wigner) phase space density of the boson emitting sources [18,9,19] and denotes the probability that a boson with momentum  $p$  is emitted from the space time point  $x$ . It specifies the one-particle momentum spectrum  $P_1(\mathbf{p}) = E_p dN/d^3p = \int d^4x S(x, p)$  as well as the two-particle correlation  $C(\mathbf{q}, \mathbf{K})$ . The r.h.s. of (2.1) has to be evaluated at  $K = \frac{1}{2}(p_1 + p_2)$  (the average momentum of the particle pair) and  $q = p_1 - p_2$  (their corresponding relative momentum) where the  $p_i$  are on-shell. The Fourier transform in (2.1) does not have a unique inverse since the four components of the relative momentum  $q$  are not independent, due to the on-shell constraint

$$q^0 = \boldsymbol{\beta} \cdot \mathbf{q}, \quad \boldsymbol{\beta} = \frac{\mathbf{K}}{K_0} \approx \frac{\mathbf{K}}{E_K}, \quad (2.2)$$

which follows from  $q \cdot K = 0$ . In practice the analysis of HBT correlation data must therefore be based on a comparison with specific models for the emission function  $S(x, K)$ , with the aim of constraining the class of “reasonable” model sources as far as possible. An important tool for this procedure are the model-independent expressions for the HBT parameters [3,4,8] which allow to calculate from an arbitrary emission function  $S$  the characteristic parameters of the two-particle correlation function  $C$  by simple quadrature. Experimentally, these HBT parameters are obtained via a multidimensional Gaussian fit to  $C(\mathbf{q}, \mathbf{K})$  in momentum space. To compute these Gaussian parameters of the (momentum) correlation function  $C$  it is sufficient to use the Gaussian approximation of the (space-time) emission function  $S$ ,

$$S(x, K) = N(\mathbf{K}) S(\bar{x}(\mathbf{K}), K) \exp \left[ -\frac{1}{2} \tilde{x}^\mu(\mathbf{K}) B_{\mu\nu}(\mathbf{K}) \tilde{x}^\nu(\mathbf{K}) \right] + \delta S(x, K), \quad (2.3)$$

neglecting  $\delta S(x, K)$  [6]. Here, the  $\tilde{x}_\mu$  denote the space-time coordinates relative to the effective “source centre”  $\bar{x}(\mathbf{K})$  for pions with momentum  $\mathbf{K}$ ,

$$\tilde{x}^\mu(\mathbf{K}) = x^\mu - \bar{x}^\mu(\mathbf{K}), \quad \bar{x}^\mu(\mathbf{K}) = \langle x^\mu \rangle, \quad (2.4)$$

and

$$(B^{-1})_{\mu\nu}(\mathbf{K}) = \langle \tilde{x}_\mu \tilde{x}_\nu \rangle \quad (2.5)$$

is the inverse of the Gaussian curvature tensor in (2.3), adjusted such that the first term in (2.3) reproduces the rms width of the full source  $S(x, K)$ . The ( $\mathbf{K}$ -dependent) expectation values in these definitions are defined as space-time averages over the emission function:

$$\langle f(x) \rangle = \frac{\int d^4x f(x) S(x, K)}{\int d^4x S(x, K)}. \quad (2.6)$$

The correction term  $\delta S$  contains information on the deviation of the emission function  $S(x, K)$  from a Gaussian form in coordinate space, i.e. on sharp edges, wiggles, secondary peaks, etc. For the class of models discussed in this paper, however, the contributions from  $\delta S$  are known to have little influence on the half width of the correlation function [6], and can be neglected. Then, the two-particle correlation function  $C(\mathbf{q}, \mathbf{K})$  can be calculated analytically from (2.1):

$$C(\mathbf{q}, \mathbf{K}) = 1 + \exp[-q^\mu q^\nu \langle \tilde{x}_\mu \tilde{x}_\nu \rangle(\mathbf{K})] . \quad (2.7)$$

It is fully determined by the  $\mathbf{K}$ -dependent second space-time moments  $(B^{-1})_{\mu\nu}$  of the source (the “effective widths”  $\langle \tilde{x}_\mu \tilde{x}_\nu \rangle(\mathbf{K})$  or “lengths of homogeneity” [4,20]).

### A. Gaussian parametrisations of the correlation function

In general, a Gaussian parametrisation of  $C(\mathbf{q}, \mathbf{K})$  is specified by selecting a particular choice of three independent components of the relative momentum  $q$  and implementing in (2.7) the on-shell constraint  $q \cdot K = 0$  accordingly. This is usually done in a Cartesian coordinate system with  $z$  along the beam axis and  $\mathbf{K}$  lying in the  $x$ - $z$ -plane. One labels the

$z$ -component of a 3-vector by  $l$  (for *longitudinal*), the  $x$ -component by  $o$  (for *outward*) and the  $y$ -component by  $s$  (for *side-ward*). The mass-shell constraint (2.2) reads

$$q^0 = \beta_\perp q_o + \beta_l q_l \quad (2.8)$$

where  $\beta_\perp = |\mathbf{K}_\perp|/K^0 \approx |\mathbf{K}_\perp|/E_K$  denotes (approximately) the velocity of the particle pair transverse to the beam direction, and  $\beta_l$  its longitudinal component.

The standard Cartesian parametrisation [3,4] of the correlation function is obtained by using (2.8) to eliminate  $q^0$  from Eq. (2.7). This determines 6 Cartesian HBT radius parameters  $R_{ij}$  in terms of the variances  $\langle \tilde{x}_\mu \tilde{x}_\nu \rangle(\mathbf{K})$  of the emission function:

$$C(\mathbf{q}, \mathbf{K}) = 1 + \exp \left[ - \sum_{i,j=s,o,l} R_{ij}^2(\mathbf{K}) q_i q_j \right],$$

$$R_{ij}^2(\mathbf{K}) = \langle (\tilde{x}_i - \beta_i \tilde{t})(\tilde{x}_j - \beta_j \tilde{t}) \rangle, \quad i, j = s, o, l. \quad (2.9)$$

For an azimuthally symmetric collision region,  $C(\mathbf{q}, \mathbf{K})$  is symmetric with respect to  $q_s \rightarrow -q_s$  [5]. Then  $R_{os}^2 = R_{sl}^2 = 0$  and [3]

$$C(\mathbf{q}, \mathbf{K}) = 1 + \exp \left[ -R_s^2(\mathbf{K}) q_s^2 - R_o^2(\mathbf{K}) q_o^2 - R_l^2(\mathbf{K}) q_l^2 - 2R_{ol}^2(\mathbf{K}) q_o q_l \right], \quad (2.10)$$

with [3,8]

$$R_s^2(\mathbf{K}) = \langle \tilde{y}^2 \rangle, \quad (2.11a)$$

$$R_o^2(\mathbf{K}) = \langle (\tilde{x} - \beta_\perp \tilde{t})^2 \rangle, \quad (2.11b)$$

$$R_l^2(\mathbf{K}) = \langle (\tilde{z} - \beta_l \tilde{t})^2 \rangle, \quad (2.11c)$$

$$R_{ol}^2(\mathbf{K}) = \langle (\tilde{x} - \beta_\perp \tilde{t})(\tilde{z} - \beta_l \tilde{t}) \rangle. \quad (2.11d)$$

An alternative way of eliminating the redundant component of  $q$  in (2.7) leads to the Yano-Koonin-Podgoretskiĭ parametrisation [5,10,11] of  $C(\mathbf{q}, \mathbf{K})$ ,

$$C(\mathbf{q}, \mathbf{K}) = 1 + \exp \left[ -R_\perp^2(\mathbf{K}) q_\perp^2 - R_\parallel^2(\mathbf{K}) (q_l^2 - (q^0)^2) - (R_o^2(\mathbf{K}) + R_\parallel^2(\mathbf{K})) (q \cdot U(\mathbf{K}))^2 \right]. \quad (2.12)$$

This is based on replacing in Eq. (2.7)  $q_o$  and  $q_s$  in terms of  $q_\perp = \sqrt{q_o^2 + q_s^2}$ ,  $q^0$ , and  $q_l$ . Here,  $U(\mathbf{K})$  is a ( $K$ -dependent) 4-velocity with only a longitudinal spatial component:

$$U(\mathbf{K}) = \gamma(\mathbf{K}) (1, 0, 0, v(\mathbf{K})), \quad \text{with } \gamma = \frac{1}{\sqrt{1-v^2}}. \quad (2.13)$$

This parametrisation has the advantage that the YKP parameters  $R_{\perp}^2(\mathbf{K})$ ,  $R_0^2(\mathbf{K})$ , and  $R_{\parallel}^2(\mathbf{K})$  extracted from such a fit do not depend on the longitudinal velocity of the observer system in which the correlation function is measured; they are invariant under longitudinal boosts. The model-independent expressions for these YKP-parameters are most conveniently given in terms of the notational shorthands [7]

$$A = \left\langle \left( \tilde{t} - \frac{\tilde{\xi}}{\beta_{\perp}} \right)^2 \right\rangle, \quad (2.14a)$$

$$B = \left\langle \left( \tilde{z} - \frac{\beta_l}{\beta_{\perp}} \tilde{\xi} \right)^2 \right\rangle, \quad (2.14b)$$

$$C = \left\langle \left( \tilde{t} - \frac{\tilde{\xi}}{\beta_{\perp}} \right) \left( \tilde{z} - \frac{\beta_l}{\beta_{\perp}} \tilde{\xi} \right) \right\rangle, \quad (2.14c)$$

where  $\tilde{\xi} \equiv \tilde{x} + i\tilde{y}$  and  $\langle \tilde{y} \rangle = \langle \tilde{x}\tilde{y} \rangle = 0$  for azimuthally symmetric sources such that  $\langle \tilde{\xi}^2 \rangle = \langle \tilde{x}^2 - \tilde{y}^2 \rangle$ . In terms of these expressions one finds<sup>1</sup>

$$v = \frac{A+B}{2C} \left( 1 - \sqrt{1 - \left( \frac{2C}{A+B} \right)^2} \right), \quad (2.15a)$$

$$R_{\parallel}^2 = B - vC, \quad (2.15b)$$

$$R_0^2 = A - vC, \quad (2.15c)$$

$$R_{\perp}^2 = \langle \tilde{y}^2 \rangle. \quad (2.15d)$$

For non-vanishing transverse pair momentum  $K_{\perp}$ , the Cartesian (2.9) and the YKP (2.12) parametrisations are equivalent and it is instructive to compare them. The Cartesian parameters can be calculated from the YKP ones via [7]

$$R_{\text{diff}}^2 = R_o^2 - R_s^2 = \beta_{\perp}^2 \gamma^2 (R_0^2 + v^2 R_{\parallel}^2), \quad (2.16a)$$

---

<sup>1</sup>These expressions are valid as long as  $(A+B)^2 > 4C^2$ , i.e. as long as expression (2.15a) for the velocity  $v$  is defined. The alternative forms of  $R_{\parallel}^2$  and  $R_0^2$  given in [7] are only valid if additionally  $A+B > 0$ . For a detailed discussion see [15].



$$R_l^2 = (1 - \beta_l^2) R_{\parallel}^2 + \gamma^2 (\beta_l - v)^2 (R_0^2 + R_{\parallel}^2) , \quad (2.16b)$$

$$R_{ol}^2 = \beta_{\perp} \left( -\beta_l R_{\parallel}^2 + \gamma^2 (\beta_l - v) (R_0^2 + R_{\parallel}^2) \right) , \quad (2.16c)$$

$$R_s^2 = R_{\perp}^2 . \quad (2.16d)$$

Later we will see that, for the explicit source models studied in this paper, in most cases the Yano-Koonin velocity  $v$  is very close to the longitudinal pair velocity  $\beta_l$ . If this is true (and one should be careful not to use the following expressions without first checking this) Eqs. (2.16b,c) simplify to

$$R_l^2 \approx R_{\parallel}^2 / \gamma^2 , \quad (2.17a)$$

$$R_{ol}^2 \approx -\beta_{\perp} \beta_l R_{\parallel}^2 . \quad (2.17b)$$

There is a slight subtlety for  $K_{\perp} = 0$ . In this limiting case, the on-shell constraint (2.2) reads  $q^0 = \beta_l q_l$  and cannot be used to eliminate in (2.7)  $q_o$  and  $q_s$  in terms of  $q_{\perp}$ ,  $q^0$  and  $q_3$ . Hence, strictly speaking, the YKP parametrisation exists only for  $K_{\perp} \neq 0$ . In practice, however, this does not lead to complications since the  $K_{\perp} \rightarrow 0$  limit is well-defined for all YKP-parameters (see Sec. IV B).

## B. Advantages and drawbacks of different Gaussian parametrizations

The relations (2.16) provide a powerful consistency check on the experimental fitting procedure of the correlation radii. They show that both parametrizations contain exactly the same spatio-temporal information. However, certain space-time characteristics of the source are more directly accessible in a particular parametrization. This is especially the case for the duration of the particle emission process, the “lifetime” of the source.

To see this we return to the expressions (2.11) for the Cartesian HBT radii. These mix spatial and temporal information on the source in a non-trivial and frame-dependent way. Their interpretation in various reference systems was analysed analytically [3–6] for a large class of (azimuthally symmetric) model emission functions and compared with the numerically calculated correlation function [6]. For these models, the difference

$$R_{\text{diff}}^2 \equiv R_o^2 - R_s^2 = \beta_{\perp}^2 \langle \tilde{t}^2 \rangle - 2\beta_{\perp} \langle \tilde{x}\tilde{t} \rangle + (\langle \tilde{x}^2 \rangle - \langle \tilde{y}^2 \rangle) \quad (2.18)$$

is dominated by the first term on the r.h.s. and thus provides access to the lifetime  $\Delta t = \sqrt{\langle \tilde{t}^2 \rangle - \langle \tilde{t} \rangle^2}$  of the source [21]. Note, however, that the definitions (2.11) and (2.18) are not Lorentz invariant, and that the lifetime  $\Delta t$  extracted from Eq. (2.18) thus depends on the analysis frame. Furthermore, in practice the term  $\beta_{\perp}^2 \langle \tilde{t}^2 \rangle$  turned out to be much smaller than the terms  $\langle \tilde{x}^2 \rangle$  and  $\langle \tilde{y}^2 \rangle$  which are the leading contributions to  $R_o^2$  and  $R_s^2$ , respectively [3–6]. As a consequence, excellent statistics of the data with very small statistical errors of  $R_o$  and  $R_s$  are required to extract the small contribution  $R_{\text{diff}}^2$ . This makes the extraction of a small source lifetime from the standard fit difficult<sup>2</sup>. Successful attempts have been reported from low-energy heavy-ion collisions (using 2-proton correlations) where the measured lifetimes are very long:  $25 \pm 15$  fm/ $c$  in Ar+Sc collisions at  $E/A = 80$  MeV [23] and  $1400 \pm 300$  fm/ $c$  in Xe+Al collisions at  $E/A = 31$  MeV [24] (the latter is the typical evaporation time of a compound nucleus). Two-pion correlations at ultra-relativistic energies ( $E/A = 200$  GeV) so far failed to yield positive evidence for a non-vanishing emission duration [25,26], except for the heaviest collision system Pb+Pb [27], but even there the effective lifetime is only a few fm/ $c$ .

For the YKP parametrization the situation is different. The parameters  $R_0$ ,  $R_{\parallel}$  and  $R_{\perp}$  are invariant under longitudinal boosts and thus independent of the analysis frame. The key to their space-time interpretation is provided by the fourth fit parameter  $v(\mathbf{K})$ . It specifies a (pair momentum dependent) longitudinal reference frame, the Yano-Koonin (YK) frame which defined by  $v = 0$  resp.  $C = 0$  (see (2.15a)), in which the space-time variances (2.15) for the YKP radius parameters simplify considerably. Especially, for certain classes of source models including the one studied below, the terms proportional to  $\langle \tilde{z}\tilde{x} \rangle$ ,  $\langle \tilde{x}\tilde{t} \rangle$ , and  $\langle \tilde{x}^2 - \tilde{y}^2 \rangle$

---

<sup>2</sup>The situation may be better for very long-lived sources which are predicted by hydrodynamics if there is a phase transition to a quark-gluon plasma and the collision fireball is initiated within a certain range of energy densities [22].

are small [5]. Neglecting these terms one obtains [5,7] in the YK frame

$$R_{\perp}^2(\mathbf{K}) = \langle \tilde{y}^2 \rangle, \quad (2.19a)$$

$$R_{\parallel}^2(\mathbf{K}) = B = \left\langle \left( \tilde{z} - \frac{\beta_l}{\beta_{\perp}} \tilde{x} \right)^2 \right\rangle - \frac{\beta_l^2}{\beta_{\perp}^2} \langle \tilde{y}^2 \rangle \approx \langle \tilde{z}^2 \rangle, \quad (2.19b)$$

$$R_0^2(\mathbf{K}) = A = \left\langle \left( \tilde{t} - \frac{1}{\beta_{\perp}} \tilde{x} \right)^2 \right\rangle - \frac{1}{\beta_{\perp}^2} \langle \tilde{y}^2 \rangle \approx \langle \tilde{t}^2 \rangle. \quad (2.19c)$$

In neighbouring frames, the Yano-Koonin velocity can be calculated with the same approximations as

$$v \approx \frac{C}{A+B} \approx \frac{\langle \tilde{z}\tilde{t} \rangle}{\langle \tilde{t}^2 \rangle + \langle \tilde{z}^2 \rangle}. \quad (2.20)$$

Note that in the YK frame the temporal structure of the source enters only in the parameter  $R_0$ . Its leading contribution is given by the time  $\Delta t(\mathbf{K}) = \sqrt{\langle \tilde{t}^2 \rangle}$  during which particles of momentum  $\mathbf{K}$  are emitted in this frame. In the YKP parametrisation  $R_0 \approx \Delta t$  is fitted directly and not obtained as the difference of two large fit parameters as in the Cartesian fit.

In practice, however, the extraction of  $R_0$  from the YKP fit is still not easy. From Eq. (2.12) it follows that in the YK frame  $R_0$  must be extracted from the  $q^0$ -dependence of the correlator. Due to the mass-shell constraint (2.2) the interesting range of  $q^0$  is limited, especially for low-momentum pairs, and the sensitivity of the fit function (2.12) to  $R_0$  is weaker than to the two other radius parameters.  $R_0$  values thus tend to come out with larger experimental error bars.

### III. A MODEL FOR A FINITE EXPANDING SOURCE

For our numerical study we have taken the model from Ref. [5] with the emission function

$$S(x, K) = \frac{M_{\perp} \cosh(\eta - Y)}{(2\pi)^3 \sqrt{2\pi(\Delta\tau)^2}} \exp \left[ -\frac{K \cdot u(x)}{T} \right] \exp \left[ -\frac{(\tau - \tau_0)^2}{2(\Delta\tau)^2} - \frac{r^2}{2R^2} - \frac{(\eta - \eta_0)^2}{2(\Delta\eta)^2} \right]. \quad (3.1)$$

The first term specifies the shape of the freeze-out hypersurface, the second one is a Lorentz-covariant Boltzmann factor encoding the assumption of local thermal equilibration superimposed by collective expansion, while the last one has a purely geometrical interpretation.

The space-time coordinates in longitudinal and temporal directions are parametrised by the space-time rapidity  $\eta = \frac{1}{2} \ln[(t+z)/(t-z)]$  and the longitudinal proper time  $\tau = \sqrt{t^2 - z^2}$ . In the transverse direction, the radius is  $r = \sqrt{x^2 + y^2}$ . Accordingly, the measure reads  $d^4x = \tau d\tau d\eta r dr d\phi$ . The time-component of the pair momentum is set to the on-shell value  $K_0 = E_K = \sqrt{m^2 + \mathbf{K}^2}$ . This approximation was studied in detail in Ref. [4] where it was shown to be acceptable. Thus the pair momentum  $K$  can be parametrised using the momentum rapidity  $Y = \frac{1}{2} \ln[(1 + \beta_l)/(1 - \beta_l)]$  and the transverse mass  $M_\perp = \sqrt{m^2 + K_\perp^2}$ ,

$$K^\mu = (M_\perp \cosh Y, K_\perp, 0, M_\perp \sinh Y). \quad (3.2)$$

We implement longitudinal and azimuthally symmetric transverse expansion of the source by parametrising the flow velocity in the form

$$u^\mu(x) = \left( \cosh \eta_l(\tau, \eta) \cosh \eta_t(r), \frac{x}{r} \sinh \eta_t(r), \frac{y}{r} \sinh \eta_t(r), \sinh \eta_l(\tau, \eta) \cosh \eta_t(r) \right). \quad (3.3)$$

For the longitudinal flow rapidity we take  $\eta_l(\tau, \eta) = \eta$  independent of  $\tau$ , i.e. we assume a Bjorken scaling profile [28]  $v_l = z/t$  in the longitudinal direction. For the transverse flow rapidity we take a linear profile of strength  $\eta_f$ :

$$\eta_t(r) = \eta_f \left( \frac{r}{R} \right). \quad (3.4)$$

The scalar product in the exponent of the Boltzmann factor generates the  $x$ - $K$ -correlation in our source. It can then be written as

$$K \cdot u(x) = M_\perp \cosh(\eta - Y) \cosh \eta_t(r) - K_\perp \frac{x}{r} \sinh \eta_t(r), \quad (3.5)$$

Please note that for non-zero transverse momentum  $K_\perp$ , a finite transverse flow breaks the azimuthal symmetry of the emission function via the second term in (3.5). For  $\eta_f = 0$ , the emission function is azimuthally symmetric for all  $K_\perp$ . Also, it then has no explicit  $K_\perp$ -dependence, and  $M_\perp$  is the only relevant scale. As will be discussed in Sec. IV D this gives rise to perfect  $M_\perp$ -scaling of the YKP radius parameters in the absence of transverse flow, which is again broken for non-zero transverse flow [29].

Besides  $\eta_f$ , the model parameters are the freeze-out temperature  $T$ , the transverse geometric (Gaussian) radius  $R$ , the average freeze-out proper time  $\tau_0$  as well as the mean proper emission duration  $\Delta\tau$ , the centre of the source rapidity distribution  $\eta_0$ , and the (Gaussian) width of the space-time rapidity profile  $\Delta\eta$ . A rough spatial picture of the source at various fixed coordinate times can be gleaned from the Figs. 1 and 2 in Ref. [30] (although their source has sharp edges whereas ours is smoothed by Gaussian profiles) and from Figs. 1 and 2 in Ref. [15]. Note that our parametrization of  $S(x, K)$  does not allow for the case of opaque sources where the emission is surface dominated [13,15]. In this case, the contribution of  $\langle \tilde{x}^2 - \tilde{y}^2 \rangle$  may become negative and large [13] which might alter the argument following (2.18). A detailed study of such opaque sources is presented in Ref. [15]. On the basis of a comparison with the preliminary data of Ref. [27] the authors of that study conclude that the source created in Pb+Pb collisions at the CERN SPS is rather transparent and not opaque; its qualitative features are well described by the model presented here [31].

We did our calculations for pions ( $m = m_{\pi^\pm} = 139 \text{ MeV}/c^2$ ) and kaons ( $m = m_{K^\pm} = 494 \text{ MeV}/c^2$ ). Resonance decays [14,16] are not discussed here but is deferred to a separate publication [17]. The calculations presented here are meant to illustrate general properties of the YKP parameters; no attempts to compare with data will be made.

#### IV. LIFETIMES AND SIZES FROM THE YKP-FIT TO THE CORRELATION FUNCTION

In this section we present a quantitative study of the YKP fit-parameters. Since the YKP-parameter  $R_\perp$  is identical to the “side” radius of the Cartesian parametrisation,  $R_\perp^2 = R_s^2 = \langle y^2 \rangle$ , its interpretation is obvious and independent of the longitudinal velocity of the reference frame. Hence we focus subsequently on the remaining three parameters  $R_0^2$ ,  $R_\parallel^2$ , and  $v$ .

Unless stated otherwise, the numerical calculations below are done with the set of source parameters  $T = 140 \text{ MeV}$ ,  $R = 3 \text{ fm}$ ,  $\Delta\eta = 1.2$ ,  $\tau_0 = 3 \text{ fm}/c$ ,  $\Delta\tau = 1 \text{ fm}/c$ .

### A. The Yano-Koonin velocity

According to Eq (2.13), the YKP fit parameter  $v$  is a longitudinal velocity. In this subsection we give a detailed discussion of the reference frame specified by  $v$  and establish its relation to several other commonly used reference frames. Their definitions are:

- **CMS**: The centre of mass frame of the fireball, specified by  $\eta_0 = 0$ .
- **LCMS** (Longitudinally CoMoving System [21]): A pion (kaon) pair-dependent frame, specified by  $\beta_l = Y = 0$ . In this frame, only the transverse velocity component of the pion (kaon) pair is non-vanishing.
- **LSPS** (Longitudinal Saddle-Point System [32]): The longitudinally moving rest frame of the point of maximal emissivity for a given pair momentum. In general, the velocity of this frame depends on the momentum of the emitted particle pair. For symmetric sources the point of maximal emissivity (“saddle point”) coincides with the “source centre”  $\bar{x}(\mathbf{K})$  defined in (2.4). In this approximation, for a source like (3.1), the LSPS velocity is given by the longitudinal component of  $u^\mu(\bar{x}(\mathbf{K}))$ .
- **YK** (Yano-Koonin frame [7]): The frame for which the YKP velocity parameter vanishes,  $v(\mathbf{K}) = 0$ . Again, this frame is in general pair momentum dependent.

These four frames are quite different in nature. The velocities (or rapidities) of the CMS and LCMS frames can be easily determined experimentally, the first from the peak in the single particle rapidity distribution, the second from the longitudinal momentum of the measured pion pair. However, the velocity of the LSPS is in a sense more interesting: from its definition it is directly related to the longitudinal expansion velocity of the source. In fact, longitudinal expansion of the source leads to a characteristic dependence of the LSPS velocity  $v_{\text{LSPS}}$  on the pair rapidity. This is most easily seen by considering two extreme fireball models:

(1) If the source does not expand, all its elements move with the same velocity (rapidity), namely that of the CMS. Then there is no kinematic difference between different parts of the fireball, and the saddle point is  $K$ -independent and given by the peak of the space-time distribution of the source. Thus the rapidity of the LSPS, defined as  $Y_{\text{LSPS}} = \frac{1}{2} \ln [(1 + v_{\text{LSPS}})/(1 - v_{\text{LSPS}})]$ , is *independent* of the pair rapidity  $Y$  and identical to the rapidity of the CMS.

This behaviour of  $Y_{\text{LSPS}}$  arises automatically if the source has no  $x-K$  correlations, i.e. if the emission function factorizes,  $S(x, K) = F(x) G(K)$ . Then all space-time characteristics of the source, including the LSPS velocity, are determined by  $F(x)$  alone and do not depend on  $K$ . Hence  $Y_{\text{LSPS}}$  is independent of  $Y$ . Factorization is, however, not necessary for this behaviour: Non-vanishing  $x-K$  correlations generated, e.g., by temperature gradients don't induce a  $Y$ -dependence of  $Y_{\text{LSPS}}$  as long as the source does not expand longitudinally.

(2) If we set in Eq. (3.1)  $\Delta\eta \rightarrow \infty$ , we recover the Bjorken model [28] for a longitudinally infinite source with boost-invariant longitudinal expansion. The only  $\eta$ -dependence then comes from the thermal Boltzmann factor, and the longitudinal saddle point obviously lies at  $\eta = Y$ . Since for the Bjorken scaling profile  $\eta$  coincides with the longitudinal fluid rapidity, this implies that in this case the rapidity of the LSPS is *identical* with the pair rapidity,  $Y_{\text{LSPS}} = Y$ , i.e. the LSPS coincides with the LCMS.

It is obvious from this discussion that knowledge of the function  $Y_{\text{LSPS}}(Y)$  would allow to distinguish between these two scenarios: A non-expanding source would yield  $Y_{\text{LSPS}}(Y) = \text{const.}$  while a source with boost-invariant longitudinal expansion gives  $Y_{\text{LSPS}}(Y) = Y$ . Realistic models are expected to lie in between these two extremes.

Unfortunately, the LSPS-velocity  $v_{\text{LSPS}}(\mathbf{K})$  cannot be measured. This is clear from its definition as the longitudinal flow velocity evaluated at the point of maximum emissivity. As discussed above, this point is approximately given by the source centre  $\bar{x}(\mathbf{K})$  which itself is unmeasurable: it drops out [7] from both the single and two-particle spectra which are invariant under a translation of the source centre (even if  $\mathbf{K}$ -dependent!). The only velocity we can measure, namely from an YKP fit of the two-particle correlator, is the Yano-Koonin

(YK) velocity  $v(\mathbf{K})$  resp. the associated rapidity  $Y_{\text{YK}} = \frac{1}{2} \ln [(1+v)/(1-v)]$ . It is therefore very gratifying to know that for sufficiently rapidly expanding systems the two velocities are always closely related (although in general not identical). In particular, we will show below that for the class of models (3.1) the function  $Y_{\text{YK}}(Y)$  shares with  $Y_{\text{LSPS}}(Y)$  the feature that it provides a direct signature for longitudinal expansion.

The close relationship between the (measurable) YK-velocity and the (theoretical) LSPS-velocity for certain source models has been known for years. In Ref. [11] a “symmetric frame” was introduced as the reference frame, in which the production process is symmetric in the beam direction. In this frame, the longitudinal extension and the lifetime of the source reach their extremal values [11]. For moving, but non-expanding azimuthally symmetric sources Podgoretskiĭ found in this way the parametrisation (2.12), with  $\mathbf{K}$ -independent parameters  $R_{\perp}$ ,  $R_{\parallel}$ , and  $R_0$ , and with what we call the Yano-Koonin velocity  $v$  being identical to the velocity of his “symmetric frame”. In this case the YK-system also coincides with the rest frame of the source as a whole (CMS) as well as with the LSPS.

That the coincidence between the YK and LSPS systems is more generally valid for sources which are symmetric around their saddle point  $\bar{x}(\mathbf{K})$  has been observed in Refs. [5,32]. It thus holds for any emission function in the Gaussian saddle-point approximation, due to the symmetry of the latter. As the following paragraph will show, differences between the YK-velocity and the velocity of the LSPS are only due to asymmetries of the source around its saddle point. Although such asymmetries usually exist for collectively expanding sources with finite geometric extension, they are generally small and can be treated perturbatively. Therefore, the YK-frame and the LSPS-frame are usually very close to each other,  $v \approx v_{\text{LSPS}}$ . From the examples above it is clear, however, that the same is not true for the LCMS (i.e. the longitudinal rest frame defined by the pair rapidity  $Y$ ), and that generally  $v \neq v_{\text{LCMS}}$ .

Let us now discuss the difference  $v - v_{\text{LSPS}}$  in more detail. If it is small, so is  $C$  when evaluated in the LSPS-frame. From Eqs. (2.20) and (2.14c) we see that then in the LSPS frame  $v$  is given by



$$v \approx \frac{C}{A+B} \approx \frac{1}{\langle \tilde{z}^2 \rangle + \langle \tilde{t}^2 \rangle} \left( \langle \tilde{z}\tilde{t} \rangle - \frac{1}{\beta_{\perp}} \langle \tilde{z}\tilde{x} \rangle - \frac{\beta_l}{\beta_{\perp}} \langle \tilde{t}\tilde{x} \rangle + \frac{\beta_l}{\beta_{\perp}^2} \langle \tilde{x}^2 - \tilde{y}^2 \rangle \right), \quad (4.1)$$

where we expanded in first order of  $\langle \tilde{z}\tilde{t} \rangle$ ,  $\langle \tilde{z}\tilde{x} \rangle$ ,  $\langle \tilde{x}^2 - \tilde{y}^2 \rangle$ . The smallness of these terms was argued in [5] and will be checked in the following subsection. The first and second term of (4.1) reflect the longitudinal asymmetry of the source around the saddle point; they vanish for sources with longitudinal reflection symmetry  $\tilde{z} \rightarrow -\tilde{z}$ . Similarly, the second and third term vanish unless the reflection symmetry  $\tilde{x} \rightarrow -\tilde{x}$  around the saddle point in the “out”-direction is broken (e.g. by transverse flow). (Asymmetry in  $t$  is needed for the first and third terms to become non-zero.) A non-zero value of the last term, finally, indicates the breaking of the “out”-“side” rotation symmetry; this can again be caused by transverse source gradients as e.g. transverse flow (see Eq. (3.5)). We conclude that the difference  $v - v_{\text{LSPS}}$  is entirely due to asymmetries of the source around the saddle point. Furthermore, we will show in Sec. IV B that the last three terms in (4.1) are small for small values of the transverse flow rapidity  $\eta_f$  and/or small values of  $K_{\perp}$ . (They vanish for  $\eta_f = 0$ .) In these limits the difference between  $v$  and  $v_{\text{LSPS}}$  is dominated by the longitudinal source asymmetry, and  $v$  is very accurately given by the (leading) first term in (4.1), see Eq. (2.20). Note that in our model the breaking of the longitudinal reflection symmetry is due to the non-symmetric rapidity profile of the emission function for  $Y \neq \eta_0$ .

For a quantitative discussion we plot in Fig. 1 the Yano-Koonin rapidity  $Y_{\text{YK}}$  as well as the difference  $Y_{\text{YK}} - Y_{\text{LSPS}}$  as functions of  $M_{\perp}$  and  $Y$ . All rapidities are given relative to the CMS. One sees that for large values of  $K_{\perp}$  the agreement of  $Y_{\text{YK}}$  with  $Y_{\text{LSPS}}$  is almost perfect. Also, in this limit both rapidities approach the value of  $Y$ , i.e. the YK and LSPS systems coincide with the LCMS. The reason for this is that for large  $K_{\perp}$  the Boltzmann term in the emission function (3.1) becomes sharply peaked around the point  $x$  where the fluid velocity agrees with the pair velocity; the geometric terms in the emission function are much smoother and can be neglected. The relevant term is the first term in Eq. (3.5), and thus the relevant variable is the transverse mass  $M_{\perp}$ . Hence this kinematic region starts for kaons at smaller values of  $K_{\perp}$  than for pions (see Fig. 1).

For small values of  $M_\perp$ , the difference  $Y_{\text{YK}} - Y_{\text{LSPS}}$  increases, and both begin to lag behind the LCMS rapidity  $Y$ . Still, the YK frame is closer to the LCMS than is the LSPS.

The fact that the YK and LSPS systems track each other so closely implies that the linear rise of the YK rapidity with the pair rapidity  $Y$  reflects nothing but a similar rise of the LSPS rapidity with  $Y$ . As argued above, the latter is a direct indication for longitudinal expansion of the source. However, it should be noted that this expansion need not necessarily be of hydrodynamic nature. The same feature would be generated by a source consisting of free-streaming pions and resonances which were created at an initial proper time  $\tau_{\text{form}}$  through a boost-invariant production mechanism [28], suffering no further re-scattering. It is easily seen that the strict correlations between coordinates and momenta in a free-streaming gas again lead to a linear dependence of the “source rapidity”  $Y_{\text{YK}}$  on the pair rapidity, with  $M_\perp$ -independent unit slope. In fact, it is possible to simulate this situation with the emission function (3.1,3.3) by setting  $T$  and  $\eta_f$  to zero, i.e. by eliminating the thermal smearing of the momenta and the transverse collective flow. (Of course, this would also result in vanishing YKP radius parameters, because pions of fixed rapidity  $Y$  can come from only a single point in the source.)

A linear rise of  $Y_{\text{YK}}$  with  $Y$  (with approximately unit slope) was recently observed by the GIBS collaboration in Dubna [12] by analysing pion correlations from Mg+Mg collisions at 4.4 A GeV/ $c$ . They interpreted their result as evidence for rapid longitudinal expansion of the source. The data were averaged over the transverse pair momentum  $K_\perp$ . The data sample was taken with a “central” trigger, but since  $^{24}\text{Mg}$  is a rather small nucleus with a large surface to volume ratio it is not clear what fraction of the participating nucleons were stopped to become part of a thermalized fireball. The strong linear increase of  $Y_{\text{YK}}$  with  $Y$  could thus also reflect to some part the free-streaming expansion of the pion sources created in the periphery of the nuclear reaction. Preliminary results of the NA49 collaboration at CERN for Pb+Pb collisions at 158 A GeV/ $c$  also show a rise of  $Y_{\text{YK}}$  with the pair rapidity  $Y$  [27]. Here, however, the  $Y$ -dependence of  $Y_{\text{YK}}$  does not appear to be quite linear, and its slope is less than 1. With all due caution with regard to the still preliminary nature of these results,

this may indicate genuine hydrodynamic longitudinal expansion at a somewhat slower rate than resulting from our longitudinal scaling profile. NA49 have also looked separately at a subsample of pairs with  $K_\perp > 300$  MeV/c, showing that for them the YK rapidity appears to rise more rapidly with  $Y$  than in the  $K_\perp$ -averaged sample, in agreement with theoretical expectations for a thermalized source (see. Fig. 1a).

The  $M_\perp$ -dependence of  $Y_{\text{YK}}$  can be understood along the same lines. Fig. 1b shows that  $Y_{\text{YK}}(Y)$  approximates  $Y$  better with increasing transverse mass. In the limit  $M_\perp \rightarrow \infty$  the bosons can be emitted only from the source element which moves exactly with the same rapidity, hence  $Y_{\text{YK}} \rightarrow Y$ . In the opposite limit  $M_\perp \rightarrow 0$  the Boltzmann factor in (3.1) becomes a smooth function of  $x$ , and the emission function is dominated by the Gaussian geometric terms. In this limit one thus expects the YK rapidity to approach the value  $Y_{\text{YK}} = \eta_0$ . The numerical results of Fig. 1b show that the value of the pion mass is already large enough for the Boltzmann part of the emission function to become important. As a result the  $M_\perp$ -dependence of  $Y_{\text{YK}}$  is weak in the entire range which can be covered by pions, and even weaker for kaons.

## B. Correction terms

In this subsection, we study quantitatively the correction terms of Eqs. (2.19) and (4.1) which may compromise the approximation (2.20) for  $v$  and the simple interpretation of  $R_\parallel$  and  $R_0$  as longitudinal and temporal widths of the emission function. Since the geometric interpretation of  $R_\parallel$  and  $R_0$  refers to the YK frame, our analysis will also be done in this frame.

Let us first focus on the central rapidity region  $Y = \eta_0$ . Then  $Y_{\text{YK}} = Y_{\text{LSPS}} = Y$ , i.e., the four reference frames listed in Sec. IV A coincide. Furthermore, the source is symmetric in the longitudinal direction and thus  $\langle \tilde{x}\tilde{z} \rangle = \langle \tilde{z}\tilde{t} \rangle \equiv 0$ . The only non-vanishing corrections thus arise from the terms  $\langle \tilde{x}\tilde{t} \rangle$  and  $\langle \tilde{x}^2 - \tilde{y}^2 \rangle$ . In Fig. 2 they are plotted as a function of  $K_\perp$  for different values of the scaling parameter  $\eta_f$  for the transverse flow. Without transverse

flow (i.e. for  $\eta_f = 0$ ) the source is azimuthally symmetric (see Eq. (3.5)) which implies  $\langle \tilde{x}^2 - \tilde{y}^2 \rangle = 0$ . Also, the source is reflection symmetric in the out-direction,  $\langle \tilde{x}\tilde{t} \rangle = 0$ . For non-zero transverse flow the correction terms are generally non-zero, and they grow with increasing  $\eta_f$ . Note that, for fixed  $\eta_f$  and  $K_\perp$ , the correction terms are considerably smaller for kaons than for pions. This can be understood as follows: as discussed after Eq. (3.5), for  $\eta_f = 0$  the source depends only on  $M_\perp$ , and thus even for non-zero transverse flow everything to zeroth order still scales with  $M_\perp$ . We will show below that for expanding sources the regions of homogeneity, which effectively contribute to the correlation function, are generically decreasing functions of  $M_\perp$ . This is thus also true for the correction terms. Since at fixed  $K_\perp$  the value of  $M_\perp$  is larger for kaons than for pions, the corresponding correction terms are smaller in absolute terms (although not necessarily relative to the leading contributions).

The  $K_\perp$ -dependence of the correction terms at non-zero transverse flow  $\eta_f \neq 0$  can also be easily understood. The rise of  $\langle \tilde{x}^2 - \tilde{y}^2 \rangle$  for increasing transverse momentum (Fig. 2a) is due to the azimuthal symmetry breaking by the second term of Eq. (3.5) which increases both with  $K_\perp$  and  $\eta_f$ . It agrees with the findings of Ref. [6] but, as pointed out in [13], contradicts the behaviour seen by Pratt in the first of Refs. [9] for an infinitesimally thin spherically expanding shell where  $\langle \tilde{x}^2 - \tilde{y}^2 \rangle$  decreases with increasing  $K_\perp$ . A similar behaviour is seen [33] in hydrodynamical simulations where freeze-out occurs along an infinitesimally thin freeze-out hypersurface; there also  $\langle \tilde{x}^2 - \tilde{y}^2 \rangle$  first decreases very rapidly with increasing  $K_\perp$ , then saturates and slightly increases again without, however, ever turning positive. The strong decrease of  $\langle \tilde{x}^2 - \tilde{y}^2 \rangle$  with  $K_\perp$  appears to be an artefact of the idealization of an infinitesimally thin expanding shell; in [15] it was shown to be much less visible for opaque sources with a finite thickness of the emitting surface layer, returning to the here observed rise already for a rather modest surface thickness.

Different from  $\langle \tilde{x}^2 - \tilde{y}^2 \rangle$ , the variance  $\langle \tilde{x}\tilde{t} \rangle$  reaches an extremum and then decreases again for very large  $K_\perp$  (Fig. 2c). This results from an interplay between the increasing breaking of the  $\tilde{x} \rightarrow -\tilde{x}$  reflection symmetry, which tends to increase the value for  $\langle \tilde{x}\tilde{t} \rangle$ , and

a decreasing homogeneity length in space-time rapidity  $\eta$  which affects the  $t = \tau \cosh \eta$  part of this variance.

In the model-independent expressions (2.19) and (4.1) for the YKP parameters, the correction terms discussed above are divided by  $\beta_\perp$  and  $\beta_\perp^2$ , respectively. From Appendix A we know that the ratios remain finite in the limit  $\beta_\perp \rightarrow 0$ . Still, the corrections to the YKP parameters could become sizeable, depending on how slowly the variances  $\langle \tilde{x}\tilde{t} \rangle$  and  $\langle \tilde{x}^2 - \tilde{y}^2 \rangle$  vanish in this limit. In Fig. 2b,d we show that the correction terms actually remain small even after dividing them by the appropriate powers of  $\beta_\perp$ . Thus, at least at mid-rapidity, the leading order approximations (2.19b,c) are seen to be generally very good. The largest correction comes from the difference  $\langle \tilde{x}^2 - \tilde{y}^2 \rangle / \beta_\perp^2$  in Eq. (2.19c). A more detailed discussion of its effects on  $R_0$  will follow in the next subsection.

We now proceed to a discussion of the correction terms for  $Y \neq \eta_0$ . We define  $Y_{\text{CM}} = Y - \eta_0$  as the rapidity of the pair in the CMS. In Fig. 3 we compare the correction terms for  $Y_{\text{CM}} = 3$  to those for  $Y_{\text{CM}} = 0$ . Of course, at  $Y_{\text{CM}} = 3$  the YK frame no longer coincides with the CMS, see Sec. IV A. Since the transverse variances are not affected by longitudinal boosts nor do they depend on  $Y$  (see Appendix A),  $\langle \tilde{x}^2 - \tilde{y}^2 \rangle$  does not change with the pair rapidity. However, at a given value of  $K_\perp$  the transverse pair velocity  $\beta_\perp = K_\perp / E_K$  becomes smaller, since  $E_K$  increases with the pair rapidity  $Y_{\text{CM}}$ . The correction term  $\langle \tilde{x}^2 - \tilde{y}^2 \rangle / \beta_\perp^2$  thus increases with  $Y_{\text{CM}}$ , especially at low  $K_\perp$ . A similar effect is seen in the plots for  $\langle \tilde{x}\tilde{t} \rangle / \beta_\perp$ . While  $\langle \tilde{x}\tilde{t} \rangle$  decreases with increasing  $Y_{\text{CM}}$ , the ratio with  $\beta_\perp$  actually increases by about a factor 2 at small  $K_\perp$ . Since in the forward rapidity region the source becomes non-symmetric under reflection  $z \rightarrow -z$ ,  $\langle \tilde{x}\tilde{z} \rangle$  and  $\langle \tilde{x}\tilde{z} \rangle / \beta_\perp$  are non-zero, but small.

We conclude this subsection with a discussion of the sensitivity of the correction terms to the longitudinal extension of the source, which is parametrised by  $\Delta\eta$ . We again put  $Y_{\text{CM}} = 0$ , so that  $\langle \tilde{x}\tilde{z} \rangle = 0$ . From the explicit expressions given in Appendix A it is clear that the transverse variances  $\langle \tilde{x}^2 - \tilde{y}^2 \rangle$  are independent of  $\Delta\eta$ . Therefore only the size of  $\langle \tilde{x}\tilde{t} \rangle$  changes. In Fig. 4 we show its  $K_\perp$ -dependence for different values of  $\Delta\eta$ . Due to our assumption of freeze-out along a hyperbola of constant proper time  $\tau_0$  (smeared by an

amount  $\Delta\tau$ ), an increase of  $\Delta\eta$  causes a larger effective extension of the source both in the  $z$  and in the time direction. This becomes especially important at small  $K_\perp$  where the geometrical factors in the emission function (3.1) play an important role. This explains the relatively large  $\Delta\eta$ -dependence of  $\langle\tilde{x}\tilde{t}\rangle$  at small  $K_\perp$  and the weaker dependence at large  $K_\perp$  where the source distribution is dominated by the Boltzmann term which does not depend on  $\Delta\eta$ .

### C. Quantitative numerical study of YKP radius parameters

In this subsection we combine the results from the previous subsection for the correction terms with the leading contributions in order to arrive at a quantitative understanding of the longitudinal and temporal YKP radius parameters  $R_\parallel$  and  $R_0$ , and in particular of their dependence on the pair momentum  $\mathbf{K}$ .

In Fig. 5 we show  $R_0$  and  $R_\parallel$  together with their approximations  $\sqrt{\langle\tilde{t}^2\rangle}$ ,  $\sqrt{\langle\tilde{z}^2\rangle}$ , for pion pairs with rapidity  $Y_{\text{CM}} = 0$  and  $Y_{\text{CM}} = 3$ , respectively, as functions of  $K_\perp$ . For vanishing transverse flow both approximations are seen to be exact, in agreement with the discussion from the previous subsection. For non-zero transverse flow the approximation  $R_\parallel \approx \sqrt{\langle\tilde{z}^2\rangle}$  remains exact for pairs with  $Y_{\text{CM}} = 0$ . The reason is that for such pairs the YK rapidity relative to the CMS is zero, and thus the longitudinal velocity  $\beta_l$  (which multiplies the correction terms in (2.19b)) of the pair in the YK frame vanishes. From Fig. 5b one sees, however, that also for forward rapidity pairs at  $Y_{\text{CM}} = 3$  the correction terms stay below 10% at all values of  $K_\perp$ .

The situation is not quite as good for  $R_0$ . Here one sees apparently strong differences between  $R_0$  and  $\sqrt{\langle\tilde{t}^2\rangle}$  as soon as the transverse flow is switched on. From Fig. 2 it is clear that the (in our case positive) correction term  $\langle\tilde{x}^2 - \tilde{y}^2\rangle$  is the culprit and dominates the difference. For a transverse flow of  $\eta_f = 0.6$  as shown in Fig. 5a this term becomes (in the experimentally accessible  $K_\perp$  range) larger than 1 (fm/c)<sup>2</sup> and thus comparable to the leading term  $\sqrt{\langle\tilde{t}^2\rangle}$ . However, the numerical results shown in this Figure actually correspond

to a rather extreme situation. First, the assumed transverse flow rapidity  $\eta_f = 0.6$  is large; the heavy ion data at AGS and CERN energies for Si- and S-induced reactions seem to require smaller values [34–36]. Second, the difference between  $R_0$  and  $\sqrt{\langle \tilde{t}^2 \rangle}$  is small at low transverse momenta and becomes large only at large  $K_\perp$ ; in that range the leading term  $\sqrt{\langle \tilde{t}^2 \rangle}$  is essentially given by the source parameter  $\Delta\tau$  (see discussion below) which in Pb+Pb and Au+Au collisions [27,30] (where  $\eta_f$  may be larger than for the smaller systems analyzed so far) seems to be bigger than the 1 fm/c assumed here<sup>3</sup>.

Fig. 5a shows that the effective source lifetime  $\Delta t = \sqrt{\langle \tilde{t}^2 \rangle}$  is a strong function of the pair momentum  $\mathbf{K}$ : it is largest at small rapidity  $Y_{\text{CM}}$  and transverse momentum  $K_\perp$  and decreases with increasing  $Y_{\text{CM}}$  and/or  $K_\perp$ . Its asymptotic value for large  $\mathbf{K}$  in the CMS is, not unexpectedly, given by the variance (A11) of the proper time distribution of our source (3.1). But why is it larger for pairs with smaller momenta  $\mathbf{K}$ ?

From Fig. 5b it is clear that the longitudinal region of homogeneity  $R_\parallel$  is a decreasing function of the pair momentum  $\mathbf{K}$ . The reason for this is the same as the similar decrease of  $R_t$  in the Cartesian fit and well understood [37] as a consequence of the strong longitudinal expansion of the source. This expansion introduces a longitudinal velocity gradient, and the longitudinal length of homogeneity is given by the inverse of this gradient multiplied by a “thermal smearing factor” [4]. The latter reflects the statistical distribution of the particle momenta around the local source fluid velocity, and for a thermal distribution the spatial region over which this thermal smearing is effective decreases with increasing pair momentum. This causes the shrinking of the longitudinal homogeneity length with  $\mathbf{K}$ .

Since for different pair momenta  $R_0$  measures the source lifetime in different YK reference

---

<sup>3</sup>If the source, unlike ours, is opaque, i.e. if the particle emission is strongly surface dominated,  $\langle \tilde{x}^2 - \tilde{y}^2 \rangle$  tends to be negative [13,15,33]. In this case, the deviation of  $R_0$  from  $\sqrt{\langle \tilde{t}^2 \rangle}$  will have the opposite sign [13,33], and  $R_0^2$  usually even turns negative for small values of  $K_\perp$ . For a detailed study we refer to [15].

frames, the freeze-out “hypersurface” will in general appear to have different shapes for pairs with different momenta. Only in our model, where freeze-out occurs at fixed proper time  $\tau_0$  (up to a Gaussian smearing with width  $\Delta\tau$ ), is it frame-independent. It is thus generally unavoidable (and here, of course, true in any frame) that freeze-out at different points  $z$  in the source will occur at different times  $t$  in the YK frame. Since a  $z$ -region of size  $R_{\parallel}$  contributes to the correlation function,  $R_{\parallel}$  determines how large a domain of this freeze-out surface (and thus how large an interval of freeze-out times in the YK frame) is sampled by the correlator. This interval of freeze-out times combines with the intrinsic Gaussian width  $\Delta\tau$  to yield the total effective duration of particle emission. It will be largest at small pair momenta where the homogeneity region  $R_{\parallel}$  is biggest, and will reduce to just the variance of the Gaussian proper time distribution at large pair momenta where the longitudinal (and transverse) homogeneity regions shrink to zero.

Another interesting feature of Fig. 5 is that at large  $K_{\perp}$  both  $R_{\parallel}$  and  $R_0$  are independent of the pair rapidity  $Y$ . This is a consequence of our boost-invariant longitudinal velocity profile and need not remain true for systems with different longitudinal expansion. As argued before, at large  $M_{\perp}$  the space-time shape of the source is dominated by the Boltzmann term and becomes insensitive to the Gaussian geometric factors. The HBT radii thus only see the local velocity gradients which in our case are invariant under longitudinal boosts. At large  $M_{\perp}$  pion pairs with different rapidities  $Y$  thus all see the same local source structure, and the YKP radii become  $Y$ -independent.

We close this subsection with a discussion of the dependence of  $R_{\parallel}$  and  $R_0$  on the other source parameters. Since the rapidity dependence does not change qualitatively from what has already been discussed, we concentrate on zero rapidity pion pairs,  $Y_{\text{CM}} = 0$ . For the transverse flow we choose a non-zero, but moderate value of  $\eta_f = 0.3$ .

In Fig. 6 we show the dependence on the longitudinal size of the source which is parametrised by  $\Delta\eta$ . One sees that at large transverse momenta neither  $R_{\parallel}$  nor  $R_0$  and  $\sqrt{\langle t^2 \rangle}$  are affected by the width  $\Delta\eta$  of the Gaussian geometric factor, in line with the arguments above. At small transverse momenta, both radii increase monotonically with  $\Delta\eta$ .



This means that, at low  $K_{\perp}$ ,  $R_{\parallel}$  becomes sensitive to the global longitudinal geometry of the source and no longer only reflects the local longitudinal velocity gradients. Fig. 6a is very interesting: for small  $\Delta\eta$  the longitudinal length of homogeneity is limited by the longitudinal geometry, and  $R_0$  never has a chance to probe a large region of the proper time freeze-out surface. Hence  $\Delta t$  is limited to the variance of the proper time distribution  $T(\tau)$  in the source (see (A2,A11)), independent of  $K_{\perp}$ . As  $\Delta\eta$  increases, at small  $K_{\perp}$  the longitudinal length of homogeneity increases too, and  $R_0$  receives an additional contribution from the time variation (in the YK rest frame) along the freeze-out surface inside a longitudinal region of size  $R_{\parallel}$ . Thus the rise of the effective source lifetime  $\Delta t$  at small  $K_{\perp}$  is an indirect measure for the longitudinal geometric size of the source. Unfortunately, the detailed quantitative dependence is model-dependent.

Fig. 7 shows what happens when the width of the proper time distribution  $T(\tau)$  (Eq. (A2)) is changed. Increasing  $\Delta\tau$  by 1 fm/c,  $R_0$  also increases by about 1 fm/c (slightly less at large  $K_{\perp}$ <sup>4</sup>), while  $R_{\parallel}$  increases more at small  $K_{\perp}$  and less at large  $K_{\perp}$ . The increase of  $R_{\parallel}$  is due to the decrease of the longitudinal velocity gradient (which for a boost-invariant profile is  $1/\tau$ ) with  $\tau$ . As the time distribution  $T(\tau)$  becomes wider, larger proper times are probed by the emitted pions resulting in larger longitudinal homogeneity regions.

Changing the average freeze-out time  $\tau_0$  rather than its spread  $\Delta\tau$  has qualitatively similar consequences (see Fig. 8), only that  $R_0$  at sufficiently large  $K_{\perp}$  again reduces to the same small variance of the time distribution  $T(\tau)$ . Note that, at small  $K_{\perp}$ ,  $R_0$  increases both with increasing  $\Delta\eta$  and increasing  $\Delta\tau$ ; this supports our claim that it is “sensitive” to the total longitudinal extension of the source  $\Delta z \simeq 2\tau_0 \sinh \Delta\eta$ . However, the relation is not linear (in particular in our numerical results a doubling of  $\Delta\eta$  is seen to have less effect

---

<sup>4</sup>Actually, the proper way of looking at this increase is by studying the variance of the function  $T(\tau)$ : according to Eq. (A11) it increases from 0.89 fm/c for  $\Delta\tau = 1$  fm/c to 1.49 fm/c for  $\Delta\tau = 2$  fm/c.

than a doubling of  $\tau_0$ ), making it hard to use in practice. It is obvious that the longitudinal velocity gradient (which decreases by a factor 2 when  $\tau_0$  is doubled) has a stronger influence on  $R_0$  and  $R_{\parallel}$  than the geometrical width in  $\eta$ .

#### D. Transverse flow, $M_{\perp}$ -scaling, and kaon interferometry

In this subsection we compare pion and kaon correlation functions. We discuss the  $M_{\perp}$ -scaling of the YKP radius parameters and its breaking by transverse collective flow. At the end of the subsection we formulate a program how to extract transverse flow from the  $M_{\perp}$ -dependence of the YKP radius parameters.

In Fig. 9 we compare, for central rapidity pairs  $Y_{\text{CM}} = 0$ , the three YKP radius parameters for pion and kaon pairs, as functions of  $K_{\perp}$ . The left column shows a source without transverse expansion, in the right column the transverse flow rapidity was set to  $\eta_f = 0.6$ . The onset of transverse flow has two qualitative effects: (i) the transverse radius acquires a  $K_{\perp}$ -dependence [6], and (ii)  $R_0$  and  $\sqrt{\langle \tilde{t}^2 \rangle}$  begin to deviate from each other, as discussed in the previous subsection. (The equality  $R_{\parallel}^2 = \langle \tilde{z}^2 \rangle$  remains exact because we are studying pion pairs at  $Y_{\text{CM}} = 0$ .) The effects of flow on  $R_{\parallel}$  and  $\sqrt{\langle \tilde{t}^2 \rangle}$  are seen to be weak, for both pions and kaons.

Note also that at small  $K_{\perp}$  the kaon radii are generically smaller than the pion radii, with or without transverse flow. This is also seen in experiment [26,38]. However, except for the change in the rest mass we have changed no parameters in the emission function, so the difference must be entirely kinematic. Indeed, it just reflects the fact that for thermalized sources like (3.1) the leading dependence on the particle rest mass is through the variable  $M_{\perp} = \sqrt{m^2 + K_{\perp}^2}$ . As discussed after Eq. (3.5) the source (3.1) depends *only* on  $M_{\perp}$  if it does not expand transversally ( $\eta_t(r) = 0$ ). In this case the correction terms in Eqs. (2.19b,c) vanish exactly, and  $R_{\perp}^2 = \langle \tilde{y}^2 \rangle$ ,  $R_{\parallel}^2 = \langle \tilde{z}^2 \rangle$ , and  $R_0^2 = \langle \tilde{t}^2 \rangle$  are also functions of  $M_{\perp}$  only. This is shown in the left column of Fig. 10 where the YKP radii for a source without transverse flow are plotted as functions of  $M_{\perp}$  and seen to exactly coincide for pions and kaons in the

common  $M_\perp$ -range. Since in the absence of transverse flow the Boltzmann factor in (3.1) has no transverse gradients (we have assumed a constant temperature  $T$ ), the transverse radius  $R_\perp$  is  $M_\perp$  independent and equal to the transverse geometric (Gaussian) radius  $R$ . It was pointed out in Refs. [4,32] that transverse temperature gradients can also cause an  $M_\perp$ -dependence of the transverse radius  $R_\perp$ ; but since the source remains in this case a function of  $M_\perp$  only, the  $M_\perp$ -scaling of the YKP radii persists; it can only be broken by transverse flow.

The breaking of the  $M_\perp$ -scaling by transverse flow is shown in the right column of Fig. 10, for  $\eta_f = 0.6$ . It has two origins: the emission function itself is no longer a function of  $M_\perp$  only (see (3.5)), and the now non-vanishing correction terms in (2.19b,c) depend on  $\beta$  and thus on both  $M_\perp$  and the rest mass  $m$ . It is obvious that the scaling violations induced by the pion-kaon mass difference are weak and require very accurate measurements. Furthermore, one may be worried that resonance decay contributions to the correlation radii [14] (which we haven't discussed here) lead also to a breaking of the  $M_\perp$  scaling, because they affect pions more than kaons, and this may make it difficult to isolate the transverse flow effects. We refer to the detailed discussion of resonance decays in the context of the model source (3.1) in Ref. [17]. That study shows, however, that their influence on the  $M_\perp$ -dependence of the transverse radius parameter  $R_\perp$  is weak [16,17]. Furthermore, resonances tend to increase all three HBT radii (in particular the effective lifetime  $R_0$ ), while the  $M_\perp$ -scaling violations from transverse flow have the opposite sign for  $R_\parallel$  and  $R_\perp, R_0$ .

Detailed dynamical studies of the freeze-out process have shown that the transverse gradients of the temperature across the freeze-out surface tend to be small [39,40]. So the experimentally observed  $M_\perp$ -dependence of the transverse radius [25–27] is presumably due to transverse flow [41]. It was shown in Ref. [6] that the strength of the  $M_\perp$ -dependence of  $R_\perp$  increases monotonously with the strength  $\eta_f$  of the transverse expansion. Alber [41] has suggested to quantify the strength of collective flow by fitting the HBT radii to a power law in  $M_\perp$ ,

$$R_{\perp}(M_{\perp}) \propto M_{\perp}^{-\alpha_{\perp}}, \quad R_{\parallel}(M_{\perp}) \propto M_{\perp}^{-\alpha_{\parallel}}, \quad (4.2)$$

and using the magnitude of the extracted (negative) power as a flow measure. He found  $\alpha_{\parallel} \simeq 0.5$  for  $R_{\parallel}$  and smaller values for  $\alpha_{\perp}$ , with a tendency to increase for larger collision systems [41]. He interpreted this as a signature for strong longitudinal and weaker transverse expansion, the latter becoming more important for larger systems.

In Fig. 11 we study the possible conclusions from such an exercise when applied to the results from our model. The left column shows double logarithmic plots for  $R_{\perp}$  and  $R_{\parallel}$  as functions of  $M_{\perp}$ . Obviously the assumption of a power law dependence is well justified for  $R_{\parallel}$  but somewhat marginal for  $R_{\perp}$ .  $R_0(M_{\perp})$  cannot be approximated by a power law at all. In the right column we show the extracted powers as a function of  $\eta_f$ , the scale parameter for the transverse flow. Since  $R_{\perp}$  is not well represented by a power law, the extracted slope depends somewhat on the fit region, as indicated for the two sets of curves in Fig. 11b. Altogether it is, however, clear that for pions the power  $\alpha_{\perp}$  increases approximately linearly with  $\eta_f$  and for kaons somewhat more strongly. But even for large transverse flow rapidities  $\eta_f \simeq 0.5$  the power remains below 0.2. In contrast, the corresponding power  $\alpha_{\parallel}$  in a fit  $R_{\parallel}(M_{\perp}) \propto M_{\perp}^{-\alpha_{\parallel}}$  is already 0.55 in the absence of transverse flow, reflecting the strong boost-invariant longitudinal expansion. (Note that the decrease of  $R_{\parallel}$  with increasing  $M_{\perp}$  is faster than the  $\sqrt{T/M_{\perp}}$ -law suggested in Ref. [37] – see also Ref. [6,42] for a discussion of this point.) As the transverse flow is switched on,  $\alpha_{\parallel}$  changes much more weakly than  $\alpha_{\perp}$ , showing that  $R_{\parallel}$  is mostly sensitive to the longitudinal flow while  $R_{\perp}$  is only affected by transverse expansion. Again, kaons are affected by the transverse flow more strongly than pions.

## V. CONCLUSIONS

We have presented a numerical study of the Yano-Koonin-Podgoretskiĭ fit parameters for the two-particle correlation function. Our starting point were the recently derived model-independent expressions for the YKP parameters in terms of second order space-time vari-

ances of the source emission function. These expressions allow for an easy evaluation of the YKP parameters as functions of the pair momentum  $\mathbf{K}$  and for detailed parameter studies. We exploited them for a class of hydrodynamic models describing locally thermalized and collectively expanding sources, and we studied the dependence of the YKP parameters on the longitudinal and temporal extension of the source as well as on its longitudinal and transverse expansion velocity.

In the context of such models it has been argued previously that in a certain approximation (which becomes exact in the absence of transverse  $x$ - $p$ -correlations of the source as, e.g., induced by transverse expansion flow) the YKP parametrisation achieves a perfect factorisation of the longitudinal and transverse spatial and the temporal extensions (“lengths of homogeneity”) of the source, in the comoving frame of the emitting fluid element. The velocity of this emitting fluid element is then given by the fourth YKP parameter (the YK velocity). Here we have shown numerically that, within these models, these features are preserved even in the presence of transverse flow. The transverse radius parameter  $R_{\perp}(\mathbf{K})$  gives the effective transverse size of the source, the longitudinal radius parameter  $R_{\parallel}(\mathbf{K})$  its effective longitudinal size, both in the local rest frame of the emitter as seen by pairs with momentum  $\mathbf{K}$ . Also, the YKP parameter  $R_0(\mathbf{K})$  provides a direct estimate of the effective emission duration for particles with momentum  $\mathbf{K}$ ; this estimate is quite accurate as long as the average transverse flow rapidity remains below 0.5 and the “lifetime parameter”  $\Delta\tau$  is not too small ( $\Delta\tau > 1 \text{ fm}/c$ ).

We also showed analytically and numerically that the YK velocity obtained from the YKP fit is indeed approximately equal to the longitudinal velocity of the emitting fluid element (the LSPS velocity), and that the small differences between these two velocities can be understood quantitatively in terms of asymmetries of the source around the point of maximum emissivity (its “saddle point”). This enables us to interpret the rise of the YK rapidity with the pair rapidity  $Y$  as a direct consequence of the longitudinal expansion of our source, and the  $M_{\perp}$ -dependence of the slope of the function  $Y_{\text{YK}}(Y)$  as a signature for the thermal smearing of the particle momenta in the fluid rest frame. In Ref. [7] we further showed that

the slope of the function  $Y_{\text{YK}}(Y)$  is nearly independent of the transverse flow rapidity  $\eta_f$ . Thus the YK rapidity is manifestly dominated by the *longitudinal* expansion and hardly affected by the transverse expansion at all. The latter causes, on the other hand, an  $M_\perp$ -dependence of the transverse radius parameter  $R_\perp$ , which in turn is completely unaffected by the longitudinal expansion. In the present model study, the YKP parametrisation thus not only leads to a factorisation of the (transverse and longitudinal) spatial and temporal aspects of the source *geometry*, but it also cleanly separates its transverse and longitudinal *dynamics*.

The sensitivity of the YKP radius parameters to the transverse expansion of the source was investigated quantitatively in Sec. IV D. While the longitudinal radius parameter  $R_\parallel$  is affected very little by the transverse flow (its strong  $M_\perp$ -dependence arises from the strong longitudinal flow), the transverse radius shows a considerable dependence on  $\eta_f$  (but none to the longitudinal flow). Furthermore, transverse flow breaks the exact  $M_\perp$ -scaling of the YKP radius parameters which we showed to exist for  $\eta_f = 0$  (see also [29]). As explained in Sec. IV D, both effects can be combined for a quantitative extraction of the mean transverse expansion velocity from the YKP radius parameters. The results from a comprehensive analysis [17] of resonance decay contributions to the correlation function indicate that they don't jeopardise such a program.

We would not like to close without remarking that the class of source models studied here is restricted in one crucial aspect: if the source is “opaque” [13], (i.e. the particle emission is strongly surface dominated rather than being distributed over the whole emission region with a Gaussian geometric weight as assumed here), the resulting differences between the variances  $\langle \tilde{x}^2 \rangle$  and  $\langle \tilde{y}^2 \rangle$  lead to much larger contributions in Eqs. (2.18), (2.19) and (4.1) than found in the present study. In Ref. [15] it is shown that this affects strongly the interpretation of measured YKP parameters, in particular of the “temporal” parameter  $R_0^2$ , which typically becomes strongly negative for small  $K_\perp$  due to the negative contribution from  $\langle \tilde{x}^2 - \tilde{y}^2 \rangle$  in this case. However, that study also shows that presently available data on YKP radii from Pb+Pb collisions [27] do not show any such indications for opaqueness of the source and

favor models with volume dominated emission. The NA44 data [43] for HBT radii from heavy ion collisions with Pb targets at the CERN SPS, which within the standard Cartesian parametrization seem to be consistent with  $R_o = R_s$ , are more difficult to interpret because of the non-trivial shape of the acceptance window of this experiment in the  $Y - K_\perp$  plane and the lack of information on the  $K$ -dependence of these parameters. Also, the important consistency relations (2.16) so far have only been checked by the NA49 collaboration [27] whose data are in qualitative agreement with the numerical results presented here [31]. A quantitative comparison with the experiments will be presented as soon as finalized data become available.

## ACKNOWLEDGMENTS

This work was supported by grants from DAAD, DFG, NSFC, BMBF and GSI. We gratefully acknowledge discussions with H. Appelshäuser, S. Chapman, D. Ferenc, P. Foka, M. Gaździcki, K. Kadija, H. Kalechofsky, M. Martin, P. Seyboth and C. Slotta. U.H. thanks the CERN Theory Group for their warm hospitality.

## APPENDIX A: SPACE-TIME MOMENTS OF THE EMISSION FUNCTION

Using cylindrical coordinates  $\tau, \eta, r, \phi$  with  $d^4x = \tau d\tau d\eta r dr d\phi$ , we can write the emission function (3.1) as

$$S(x, K) d^4x = T(\tau) P(r, \phi) H(r, \eta) d\tau d\eta dr d\phi, \quad (\text{A1})$$

with

$$T(\tau) = \frac{\tau}{\sqrt{2\pi(\Delta\tau)^2}} \exp\left(-\frac{(\tau - \tau_0)^2}{2(\Delta\tau)^2}\right), \quad (\text{A2})$$

$$P(r, \phi) = \frac{1}{2\pi} e^{b(r) \cos \phi}, \quad (\text{A3})$$

$$H(r, \eta) = \frac{r}{(2\pi)^2} \exp\left(-\frac{r^2}{2R^2} - \frac{(\eta - \eta_0)^2}{2(\Delta\eta)^2}\right) M_\perp \cosh(\eta - Y) e^{-a(r) \cosh(\eta - Y)}, \quad (\text{A4})$$

where we defined

$$a(r) = \frac{M_{\perp}}{T} \cosh \eta_t(r), \quad (\text{A5})$$

$$b(r) = \frac{K_{\perp}}{T} \sinh \eta_t(r). \quad (\text{A6})$$

The  $\phi$  and  $\tau$  integrations can be done analytically. We use

$$\int_0^{2\pi} \frac{d\phi}{2\pi} e^{b \cos \phi} \cos(n\phi) = I_n(b) \quad (\text{A7})$$

and define

$$T_0 = \langle 1 \rangle_{\tau} = \int_{-\infty}^{\infty} T(\tau) d\tau = \tau_0, \quad (\text{A8})$$

$$T_1 = \langle \tau \rangle_{\tau} = \int_{-\infty}^{\infty} \tau T(\tau) d\tau = \tau_0^2 + (\Delta\tau)^2, \quad (\text{A9})$$

$$T_2 = \langle \tau^2 \rangle_{\tau} = \int_{-\infty}^{\infty} \tau^2 T(\tau) d\tau = \tau_0^3 + 3\tau_0(\Delta\tau)^2. \quad (\text{A10})$$

The variance of the  $\tau$ -distribution  $T(\tau)$  is

$$\langle \tau^2 \rangle_{\tau} - \langle \tau \rangle_{\tau}^2 = (\Delta\tau)^2 \left( 1 - \left( \frac{\Delta\tau}{\tau_0} \right)^2 \right). \quad (\text{A11})$$

Defining further

$$\langle f(r, \eta) \rangle_* = \frac{\int_0^{\infty} dr \int_{-\infty}^{\infty} d\eta H(r, \eta) I_0(b(r)) f(r, \eta)}{\int_0^{\infty} dr \int_{-\infty}^{\infty} d\eta H(r, \eta) I_0(b(r))} \quad (\text{A12})$$

we find for the non-vanishing moments up to second order

$$\langle x^2 \rangle = \frac{1}{2} \left\langle r^2 \left( 1 + \frac{I_2(b(r))}{I_0(b(r))} \right) \right\rangle_*, \quad (\text{A13})$$

$$\langle y^2 \rangle = \frac{1}{2} \left\langle r^2 \left( 1 - \frac{I_2(b(r))}{I_0(b(r))} \right) \right\rangle_*, \quad (\text{A14})$$

$$\langle z^2 \rangle = \frac{T_2}{T_0} \langle \sinh^2 \eta \rangle_*, \quad (\text{A15})$$

$$\langle t^2 \rangle = \frac{T_2}{T_0} \langle \cosh^2 \eta \rangle_*, \quad (\text{A16})$$

$$\langle x \rangle = \left\langle r \frac{I_1(b(r))}{I_0(b(r))} \right\rangle_*, \quad (\text{A17})$$

$$\langle z \rangle = \frac{T_1}{T_0} \langle \sinh \eta \rangle_*, \quad (\text{A18})$$



$$\langle t \rangle = \frac{T_1}{T_0} \langle \cosh \eta \rangle_* , \quad (\text{A19})$$

$$\langle xt \rangle = \frac{T_1}{T_0} \left\langle r \cosh \eta \frac{I_1(b(r))}{I_0(b(r))} \right\rangle_* , \quad (\text{A20})$$

$$\langle zt \rangle = \frac{T_2}{T_0} \langle \sinh \eta \cosh \eta \rangle_* , \quad (\text{A21})$$

$$\langle xz \rangle = \frac{T_1}{T_0} \left\langle r \sinh \eta \frac{I_1(b(r))}{I_0(b(r))} \right\rangle_* . \quad (\text{A22})$$

For  $\eta_f \neq 0$  the  $\langle \dots \rangle_*$ -averages have to be done numerically. For convenience we also give

$$\langle \tilde{x}\tilde{t} \rangle = \frac{T_1}{T_0} \left[ \left\langle r \cosh \eta \frac{I_1(b(r))}{I_0(b(r))} \right\rangle_* - \left\langle r \frac{I_1(b(r))}{I_0(b(r))} \right\rangle_* \langle \cosh \eta \rangle_* \right] , \quad (\text{A23})$$

$$\langle \tilde{x}^2 - \tilde{y}^2 \rangle = \left\langle r^2 \frac{I_2(b(r))}{I_0(b(r))} \right\rangle_* - \left\langle r \frac{I_1(b(r))}{I_0(b(r))} \right\rangle_*^2 . \quad (\text{A24})$$

Please note that for small arguments  $I_n(b) \sim b^n$ . Thus for small  $\eta_f$  and/or  $K_\perp$ ,  $\langle \tilde{x}\tilde{t} \rangle$  and  $\langle \tilde{x}^2 - \tilde{y}^2 \rangle$  vanish linearly and quadratically, respectively.

## REFERENCES

- \* On leave of absence from Institute of Particle Physics, Hua-Zhong Normal University, Wuhan, China.
- [1] M. Gyulassy, S.K. Kauffmann, and L.W. Wilson, Phys. Rev. **C20**, 2267 (1979).
  - [2] D. Boal, C.K. Gelbke and B. Jennings, Rev. Mod. Phys. **62**, 553 (1990).
  - [3] S. Chapman, P. Scotto, and U. Heinz, Phys. Rev. Lett. **74**, 4400 (1995).
  - [4] S. Chapman, P. Scotto, and U. Heinz, Heavy Ion Physics **1**, 1 (1995).
  - [5] S. Chapman, J.R. Nix, and U. Heinz, Phys. Rev. **C52**, 2694 (1995).
  - [6] U.A. Wiedemann, P. Scotto and U. Heinz, Phys. Rev. **C53**, 918 (1996).
  - [7] U. Heinz, B. Tomášik, U.A. Wiedemann, and Y.-F. Wu, Phys. Lett. **B382**, 181 (1996).
  - [8] M. Herrmann and G.F. Bertsch, Phys. Rev. **C51**, 328 (1995).
  - [9] S. Pratt, Phys. Rev. Lett. **53**, 1219 (1984); Phys. Rev. **D33**, 1314 (1986).
  - [10] F. Yano and S. Koonin, Phys. Lett. **78B**, 556 (1978).
  - [11] M.I. Podgoretskiĭ , Sov. J. Nucl. Phys. **37**, 272 (1983).
  - [12] GIBS Coll., M.Kh. Anikina et al., Dubna preprint JINR E1-95-311 (1995).
  - [13] H. Heiselberg and A.P. Vischer, Los Alamos eprint archive nucl-th/9609022 and nucl-th/9703030.
  - [14] B.R. Schlei, U. Ornik, M. Plümer, and R. Weiner, Phys. Lett. **B293**, 275 (1992); J. Bolz, U. Ornik, M. Plümer, B.R. Schlei, and R. Weiner, Phys. Lett. **B300**, 404 (1993); and Phys. Rev. **D47**, 3860 (1993).
  - [15] B. Tomášik and U. Heinz, in preparation.
  - [16] U. Heinz, Nucl. Phys. **A610**, 264c (1996).

- [17] U.A. Wiedemann and U. Heinz, *Resonance decay contributions to HBT correlation radii*,  
Los Alamos eprint archive nucl-th/9611031.
- [18] E. Shuryak, Phys. Lett. B**44**, 387 (1973); Sov. J. Nucl. Phys. **18**, 667 (1974).
- [19] S. Chapman and U. Heinz, Phys. Lett. B**340**, 250 (1994).
- [20] S.V. Akkelin and Y.M. Sinyukov, Phys. Lett. B**356**, 525 (1995).
- [21] T. Csörgő and S. Pratt, in *Proceedings of the Workshop on Relativistic Heavy Ion Physics at Present and Future Accelerators*, Budapest, 1991, edited by T. Csörgő et al. (MTA KFKI Press, Budapest, 1991), p. 75.
- [22] D.H. Rischke and M. Gyulassy, Nucl. Phys. A**607**, 479 (1996).
- [23] M.A. Lisa et al., Phys. Rev. Lett. **71**, 2863 (1993).
- [24] M.A. Lisa et al., Phys. Rev. C**49**, 2788 (1994).
- [25] NA35 Coll., T. Alber et al., Z. Phys. C**66**, 77 (1995);  
NA35 Coll., T. Alber et al., Phys. Rev. Lett. **74**, 1303 (1995).
- [26] NA44 Coll., H. Beker et al., Phys. Rev. Lett. **74**, 3340 (1995).
- [27] K. Kadija (NA49 Coll.), Nucl. Phys. A**610**, 248c (1996).
- [28] J.D. Bjorken, Phys. Rev. D**27**, 140 (1983).
- [29] U. Heinz, B. Tomášik, U.A. Wiedemann, and Y.-F. Wu, Heavy Ion Physics **4**, 249 (1996).
- [30] S. Chapman and J.R. Nix, Phys. Rev. C**54**, 866 (1996).
- [31] U. Heinz, in *QCD Phase Transitions*, ed. by H. Feldmeier et al., Proceedings of the 25th International Workshop on Gross Properties of Nuclei and Nuclear Excitations, Hirschegg, Austria, Jan. 13-18, 1997; GSI Report ISSN 0720-8715, Los Alamos eprint archive nucl-th/9701054.

- [32] T. Csörgő and B. Lörstad, Phys. Rev. C**54**, 1396 (1996); and Nucl. Phys. A**590**, 465c (1995).
- [33] B. Schlei and U. Heinz, in preparation.
- [34] K.S. Lee, U. Heinz, and E. Schnedermann, Z. Phys. C**48**, 525 (1990); E. Schnedermann and U. Heinz, Phys. Rev. Lett. **69**, 2908 (1992); E. Schnedermann, J. Sollfrank, and U. Heinz, Phys. Rev. C**48**, 2462 (1993).
- [35] P. Braun-Munzinger, J. Stachel, J.P. Wessels, and N. Xu, Phys. Lett. B**344**, 43 (1994); J. Stachel, Nucl. Phys. A**610**, 509c (1996).
- [36] N. Herrmann (FOPI Coll.), Nucl. Phys. A**610**, 49c (1996).
- [37] A.N. Makhlin and Yu.M. Sinyukov, Z. Phys. C**39**, 69 (1988).
- [38] E802 Coll., V. Cianciolo et al., Nucl. Phys. A**590**, 459c (1995).
- [39] U. Heinz, K.S. Lee, and E. Schnedermann, in *The Nuclear Equation of State*, edited by W. Greiner and H. Stöcker, NATO ASI Series 216B, p. 385 (Plenum, New York, 1990).
- [40] U. Mayer, PhD thesis, University of Regensburg, 1995, unpublished.
- [41] NA49 Coll., T. Alber et al., Nucl. Phys. A**590**, 453c (1995); T. Alber, PhD thesis, MPI für Physik, München (1995), unpublished.
- [42] Yu.M. Sinyukov, S.V. Akkelin, and A.Yu. Tolstykh, Nucl. Phys. A**610**, 278c (1996).
- [43] A. Franz (NA44 Coll.), Nucl. Phys. A**610**, 240c (1996).

## FIGURES

FIG. 1. (a) The rapidity of the YK frame as a function of the pair rapidity  $Y$  (both measured in the source CMS), for pions (solid) and kaons (dashed) and for transverse momenta  $K_\perp = 1$  MeV and  $K_\perp = 1000$  MeV. The transverse flow was set to  $\eta_f = 0.3$ . (b) Same as (a), but shown as a function of  $M_\perp$  for different values of  $Y$ . (c) The difference  $Y_{\text{YK}} - Y_{\text{LSPS}}$  (see text), plotted in the same way as (a). (d) Same as (c), but shown as a function of  $M_\perp$  for different values of  $Y$ .

FIG. 2. The correction terms  $\langle \tilde{x}^2 - \tilde{y}^2 \rangle$  (a) and  $\langle \tilde{x}\tilde{t} \rangle$  (c), for pairs with  $Y = 0$  in the CMS, as functions of  $K_\perp$  for different values of  $\eta_f$ . The third correction term  $\langle \tilde{x}\tilde{z} \rangle$  vanishes at  $Y = 0$ . Solid (dashed) lines refer to pion (kaon) pairs. Figures (b) and (d) show the same quantities, but scaled by the appropriate inverse powers of  $\beta_\perp$  (see text).

FIG. 3. Same as Fig. 2, but now for a fixed transverse flow  $\eta_f = 0.3$  and pions only, but for two different pair rapidities,  $Y_{\text{CM}} = 0$  (solid) and  $Y_{\text{CM}} = 3$  (dashed). The curves were evaluated in the YK frame.

FIG. 4. Dependence of the correction term  $\langle \tilde{x}\tilde{t} \rangle(K_\perp)$  on the longitudinal width parameter  $\Delta\eta$ , for pion pairs with  $Y_{\text{CM}} = 0$ .

FIG. 5. (a)  $R_0$  and  $\sqrt{\langle \tilde{t}^2 \rangle}$  as functions of  $K_\perp$  for  $\eta_f = 0$  and  $\eta_f = 0.6$ , for pion pairs with rapidity  $Y_{\text{CM}} = 0$  and  $Y_{\text{CM}} = 3$ . The lifetime  $\sqrt{\langle \tilde{t}^2 \rangle}$  is evaluated in the YK rest frame. (b) Same as (a), but for  $R_\parallel$  and the longitudinal length of homogeneity  $\sqrt{\langle \tilde{z}^2 \rangle}$  in the YK rest frame. For  $Y_{\text{CM}} = 0$ ,  $R_\parallel$  and  $\sqrt{\langle \tilde{z}^2 \rangle}$  agree exactly because  $\beta_l = 0$  in the YK frame.

FIG. 6. (a)  $R_0$  and  $\sqrt{\langle \tilde{t}^2 \rangle}$  as functions of  $K_\perp$ , for different longitudinal gaussian widths  $\Delta\eta$ . The diagrams are for pion pairs with  $Y_{\text{CM}} = 0$  and for transverse flow  $\eta_f = 0.3$ . The lifetime  $\sqrt{\langle \tilde{t}^2 \rangle}$  is evaluated in the YK rest frame which coincides here with the CMS and the LCMS. (b) Same as (a), but for  $R_\parallel$ . Since  $Y_{\text{CM}} = 0$ ,  $R_\parallel$  and the longitudinal length of homogeneity in the YK frame  $\sqrt{\langle \tilde{z}^2 \rangle}$  agree exactly.

FIG. 7. Same as Fig. 6, but for different widths  $\Delta\tau$  of the proper time distribution in the source.

FIG. 8. Same as Fig. 6, but for different average freeze-out times  $\tau_0$ .

FIG. 9. The YKP radii  $R_\perp$  (top row),  $R_\parallel$  (middle row), and  $R_0$  (bottom row), for  $Y_{\text{CM}} = 0$  pion (solid) and kaon (dashed) pairs, as functions of  $K_\perp$ . Left column: no transverse flow. Right column: transverse flow  $\eta_f = 0.6$ . In the lower right panel we also show the effective lifetime in the YK frame  $\sqrt{\langle \tilde{t}^2 \rangle}$  for comparison. For more discussion see text.

FIG. 10. Same as Fig. 9, but plotted as functions of  $M_\perp$ .

FIG. 11. (a)  $R_\perp$  as a function of  $M_\perp$  at  $Y_{\text{CM}} = 0$ , for pions (solid) and kaons (dashed) and different transverse flow rapidities  $\eta_f$ . (b) The scaling coefficient  $\alpha_\perp$  defined by  $R_\perp \approx M_\perp^{-\alpha_\perp}$  for pions (solid) and kaons (dashed) as a function of the transverse flow rapidity  $\eta_f$ . The different results obtained by fitting in the regions  $M_\perp - m < 500 \text{ MeV}/c^2$  and  $M_\perp - m < 1000 \text{ MeV}/c^2$  are shown separately. (c) Same as (a), but for  $R_\parallel$ . (d) Same as (b), but for  $\alpha_\parallel$ .

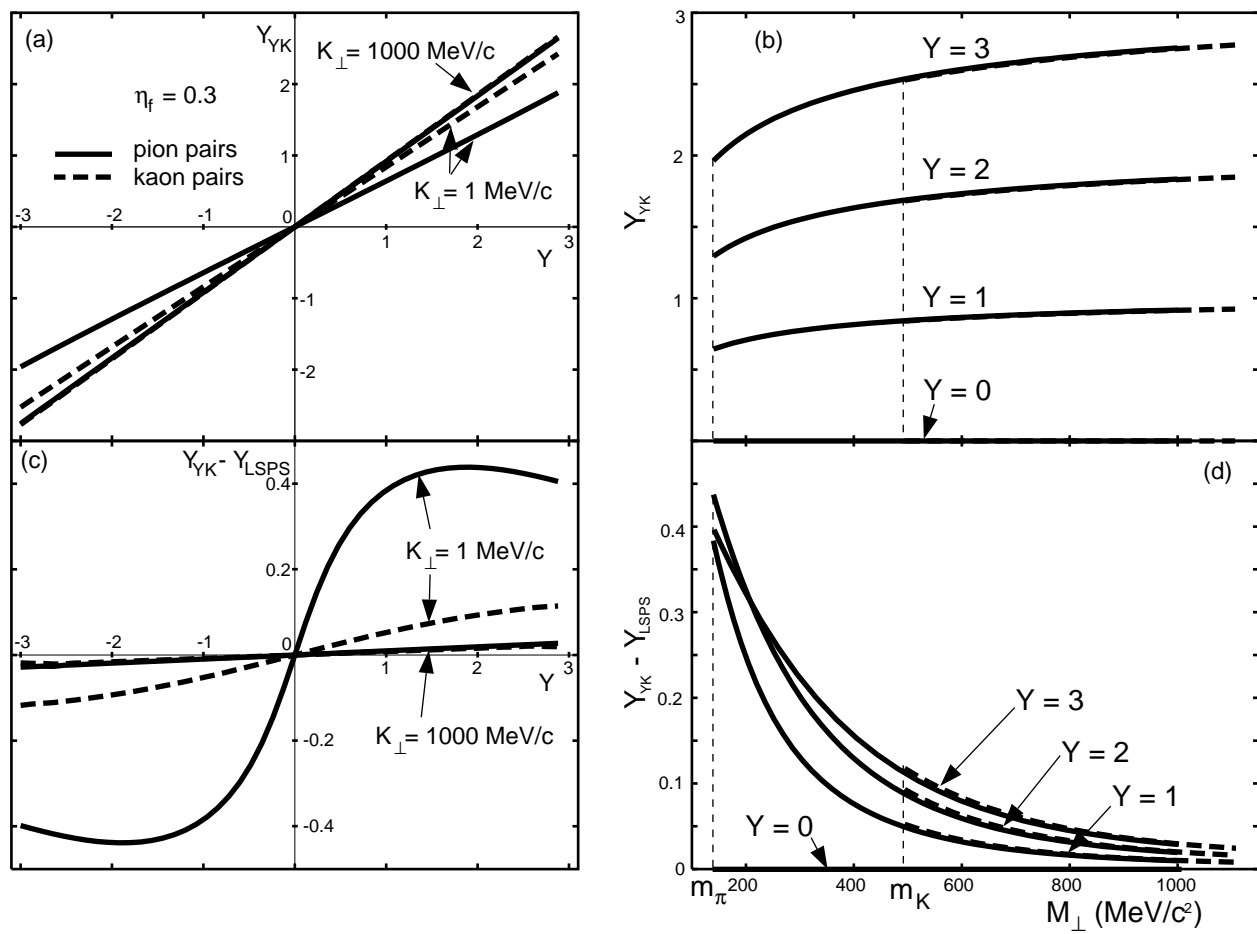


Fig.1

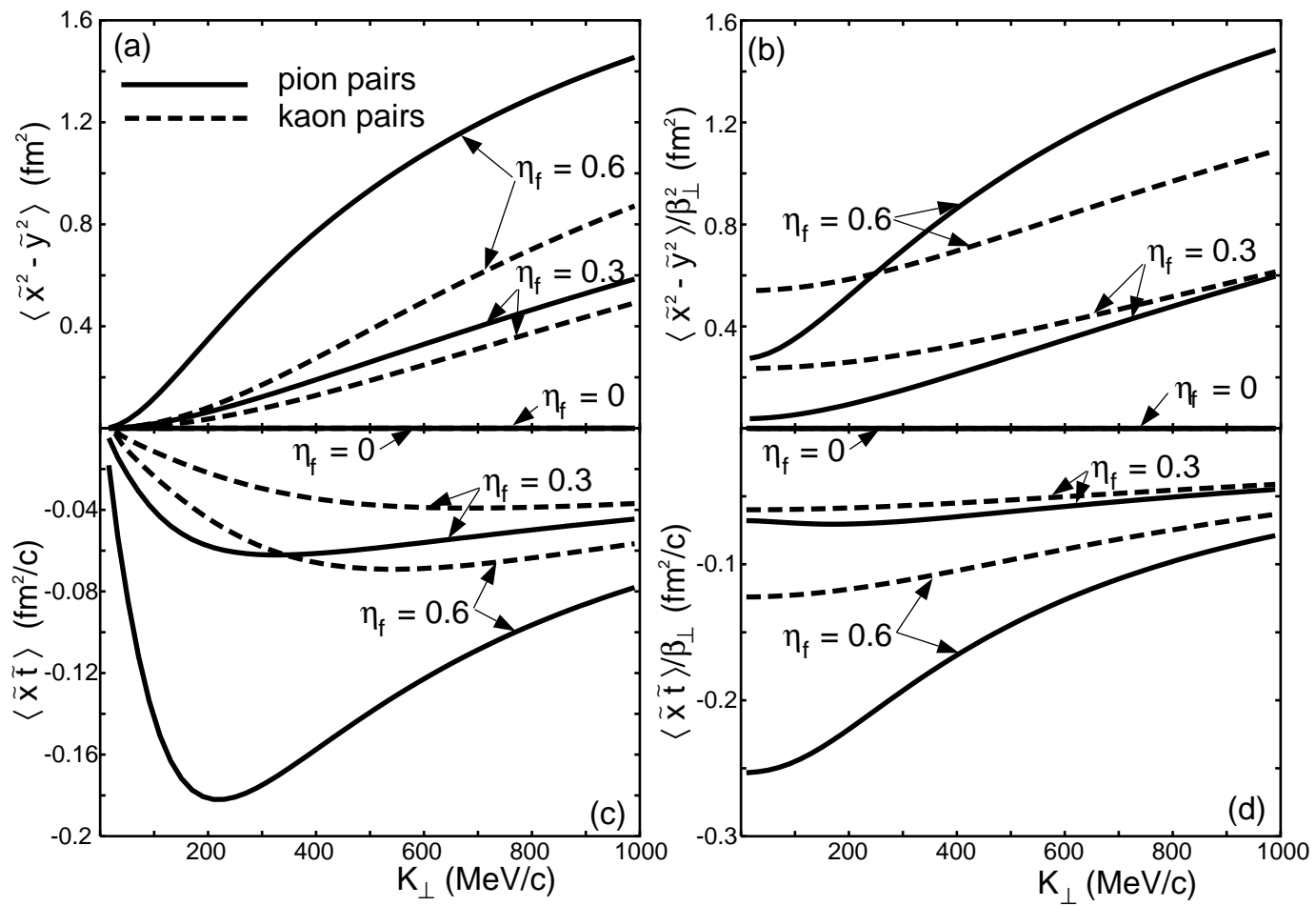


Fig.2



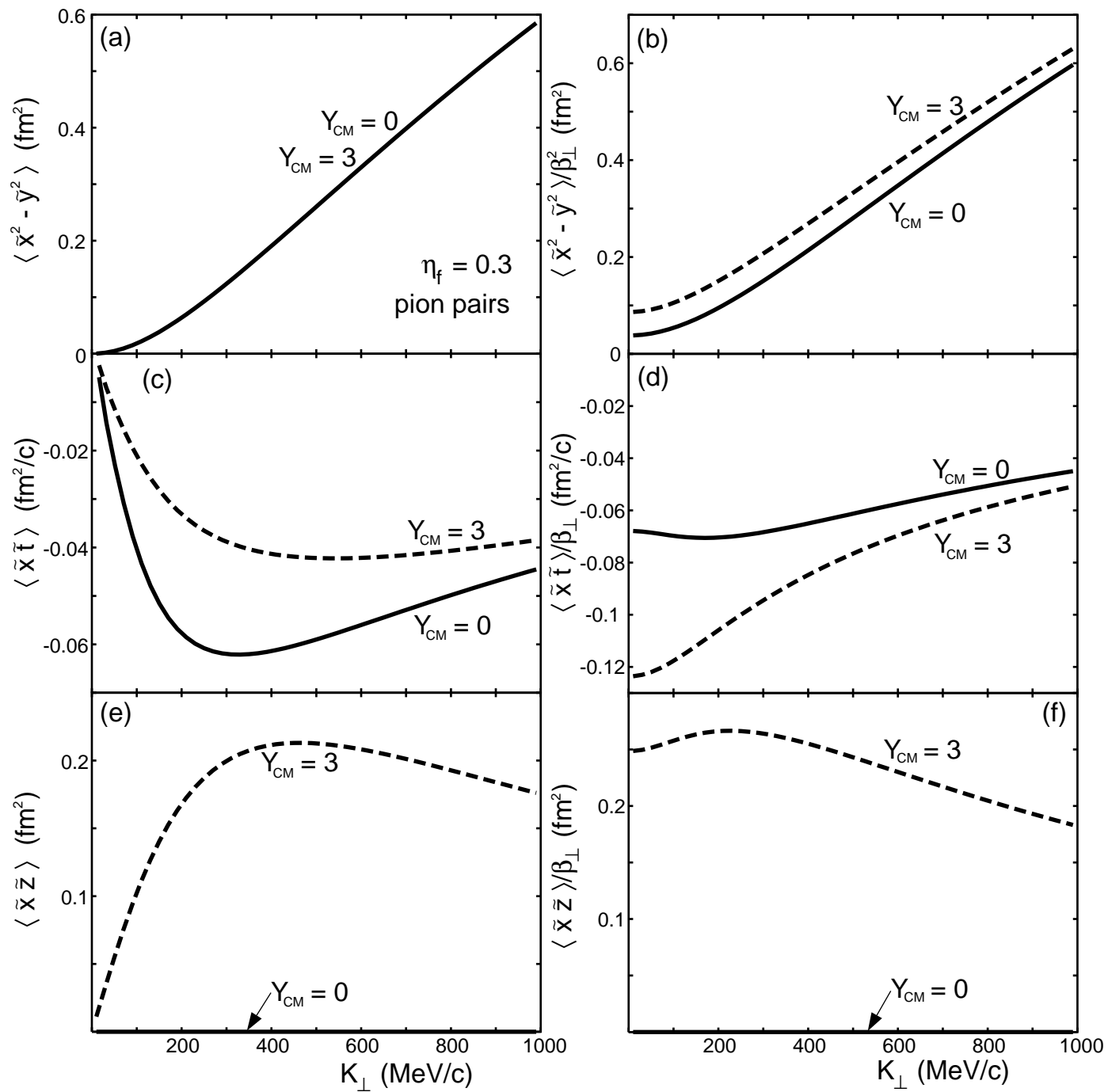


Fig.3

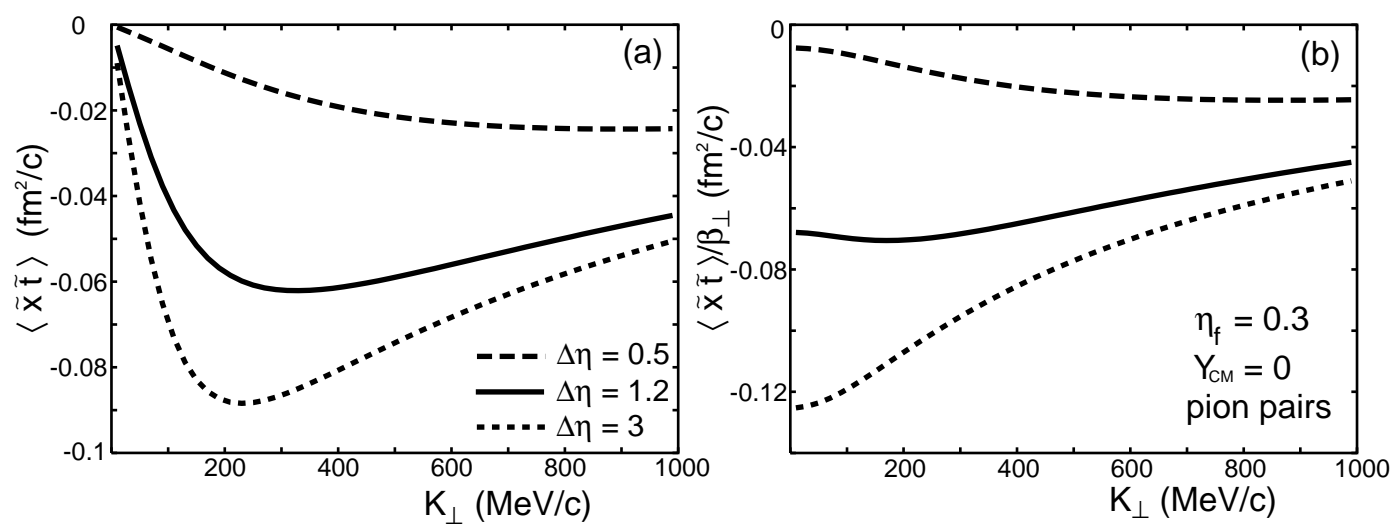


Fig.4

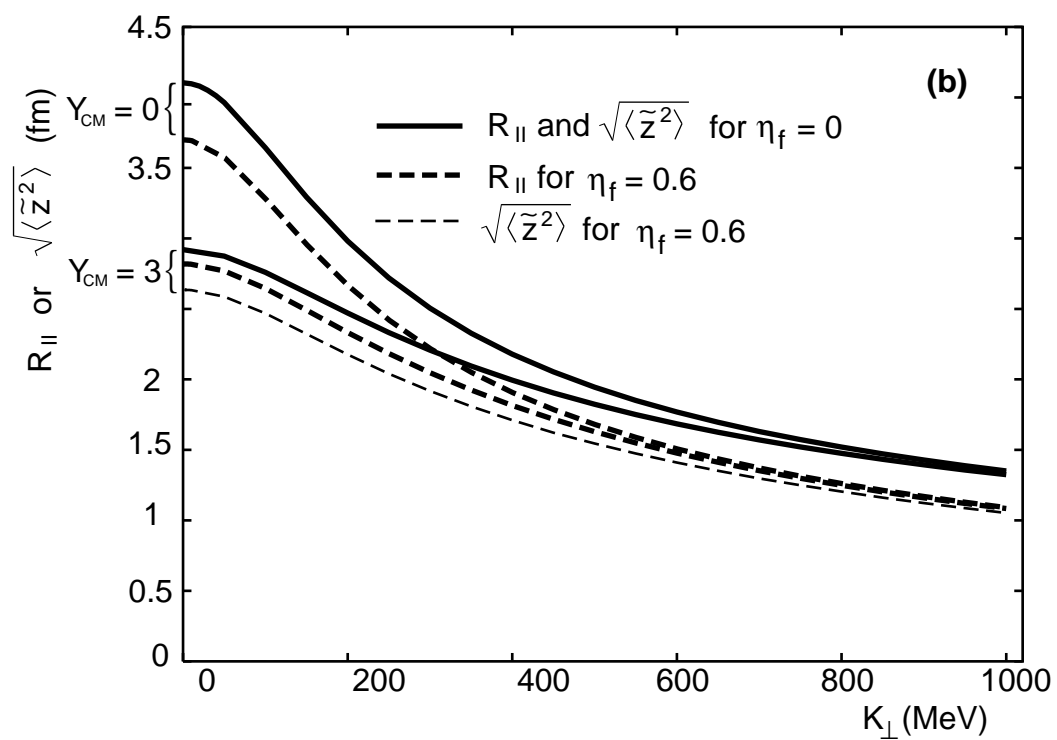
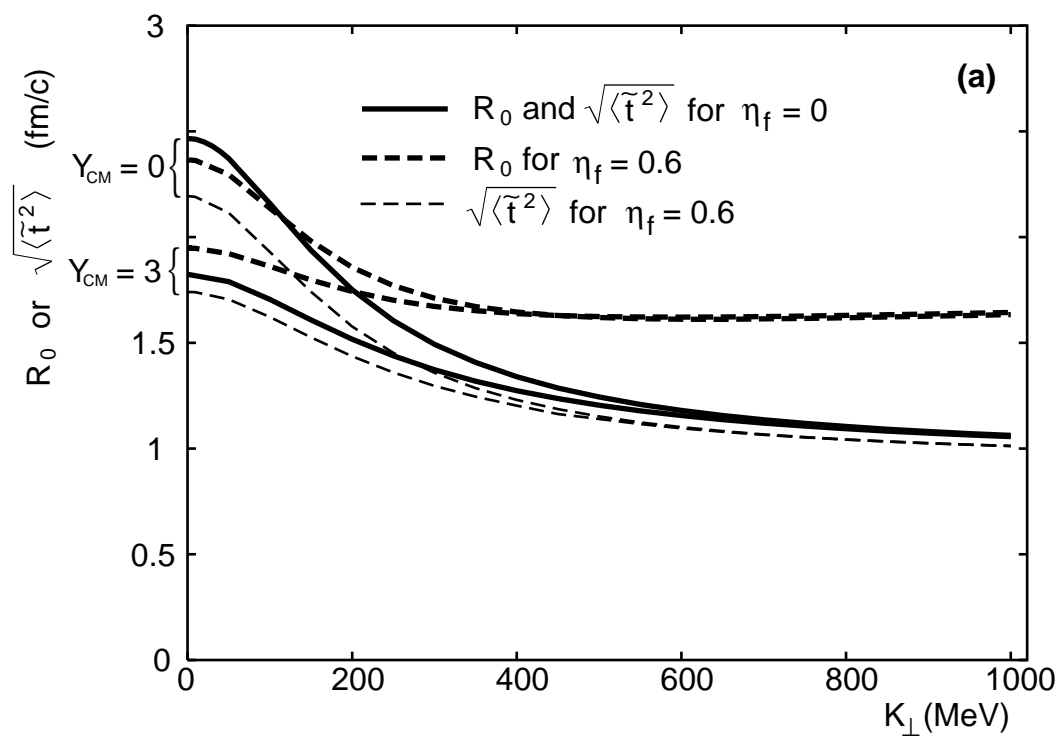


Fig.5

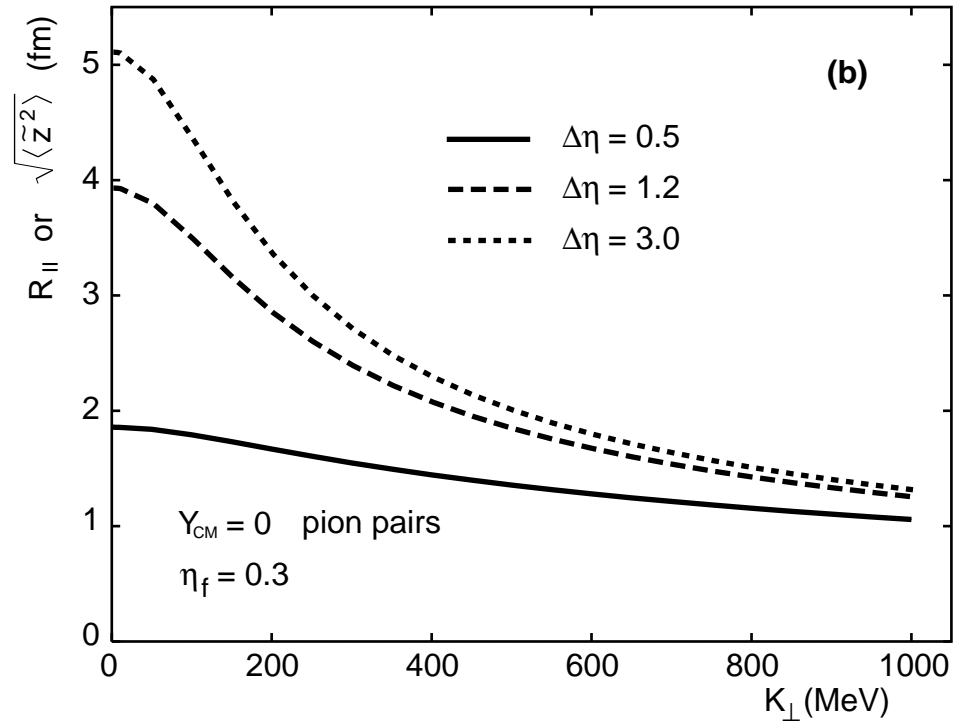
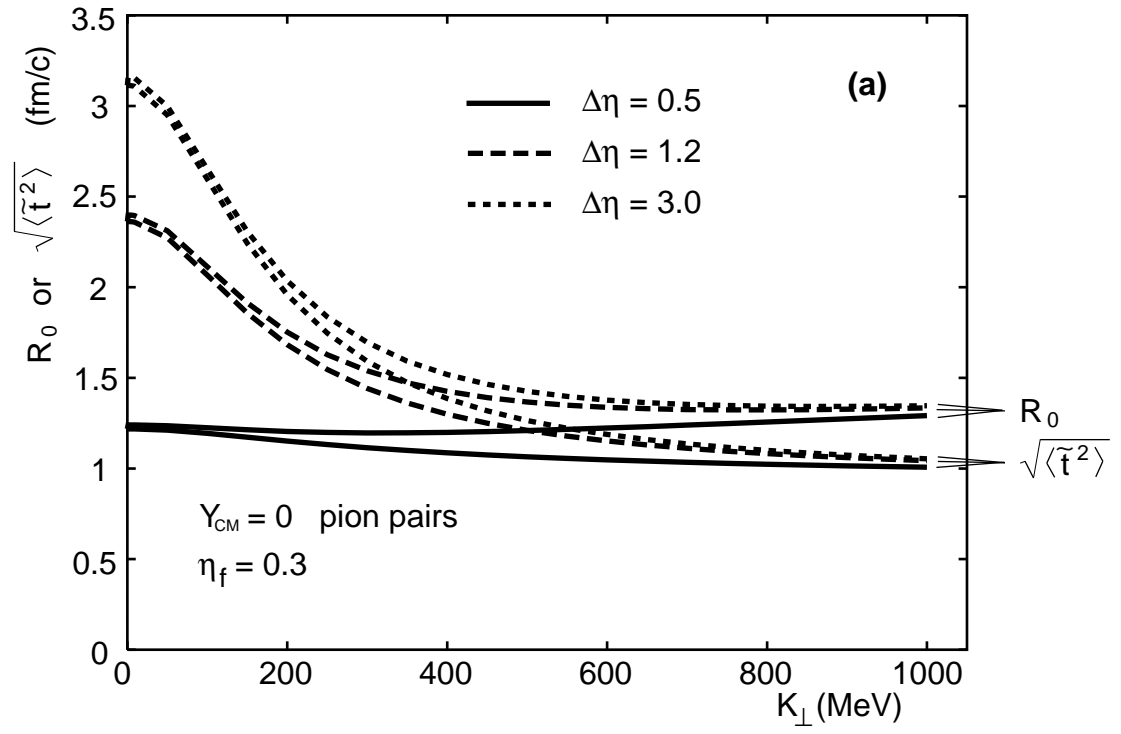


Fig.6

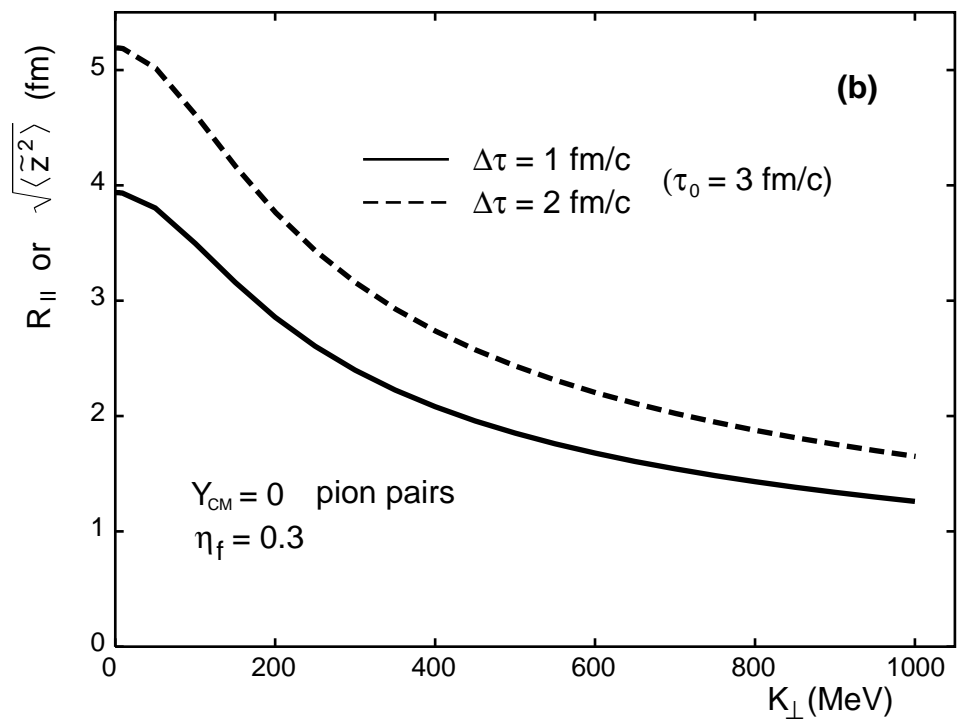
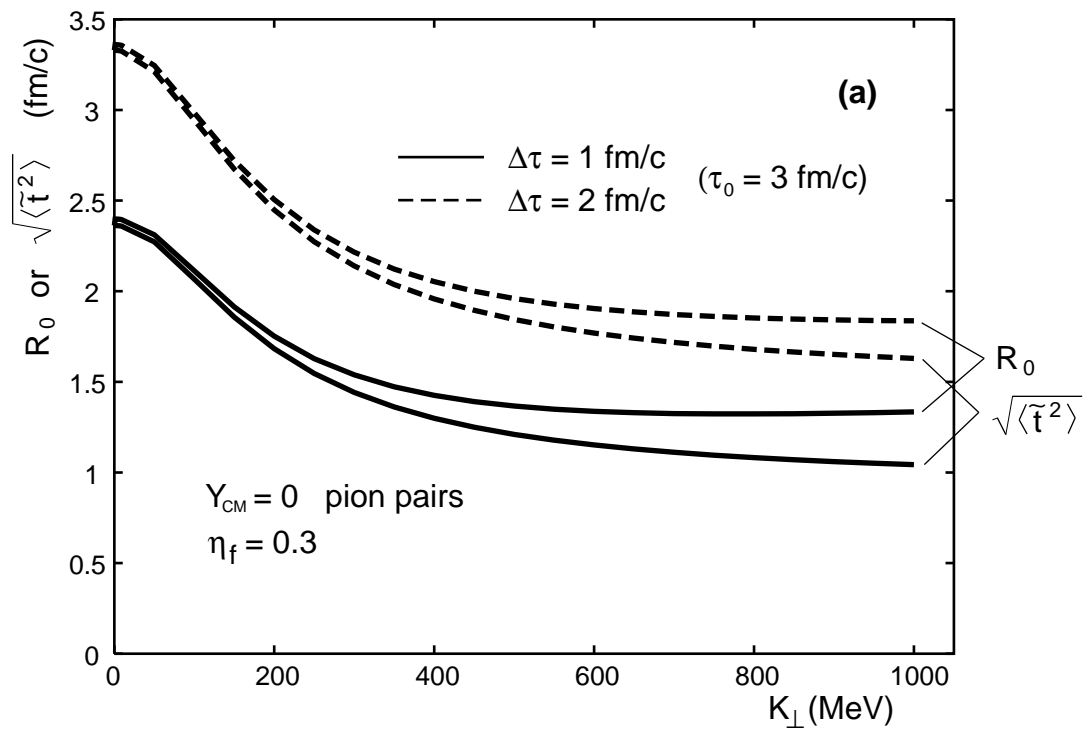


Fig.7

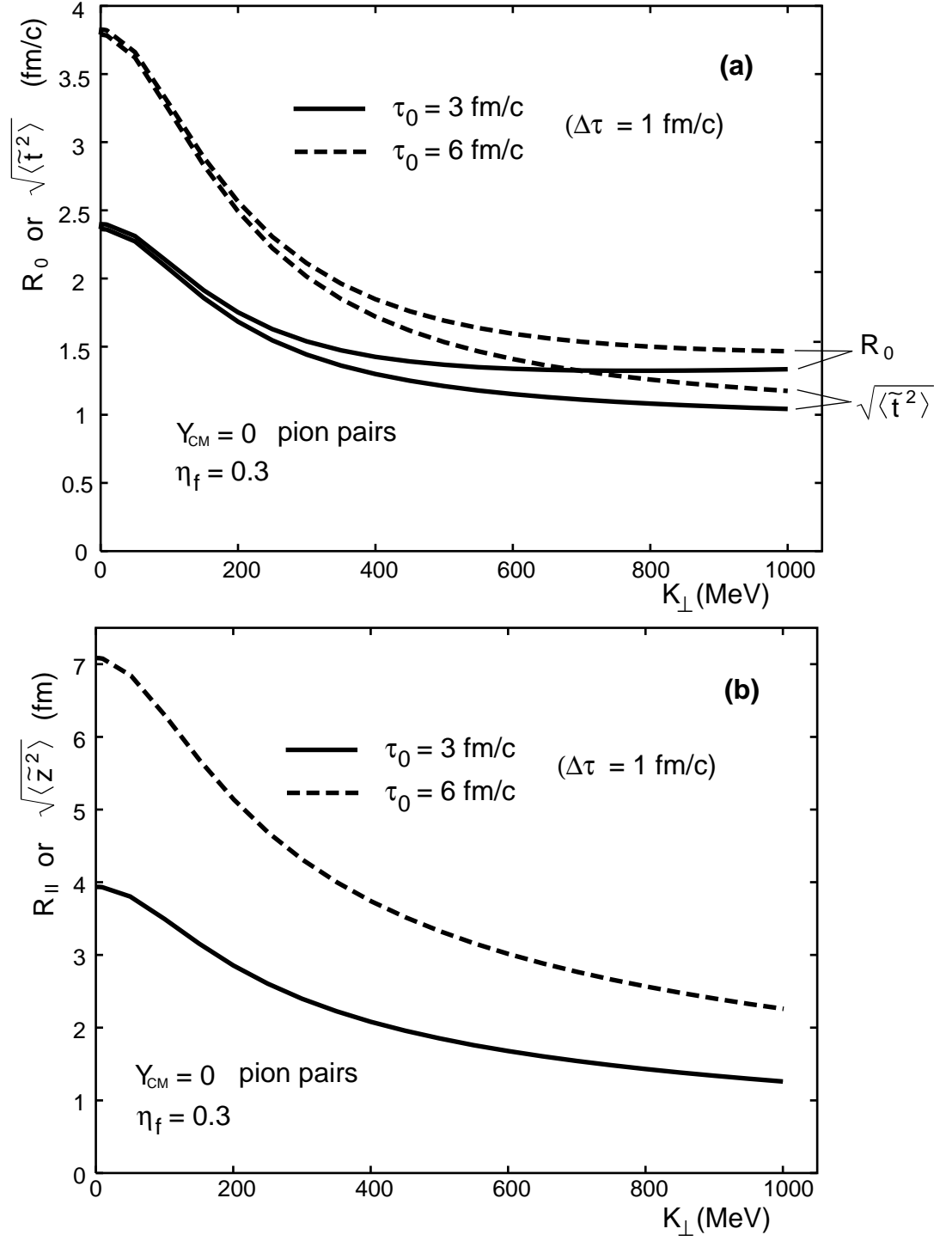


Fig.8

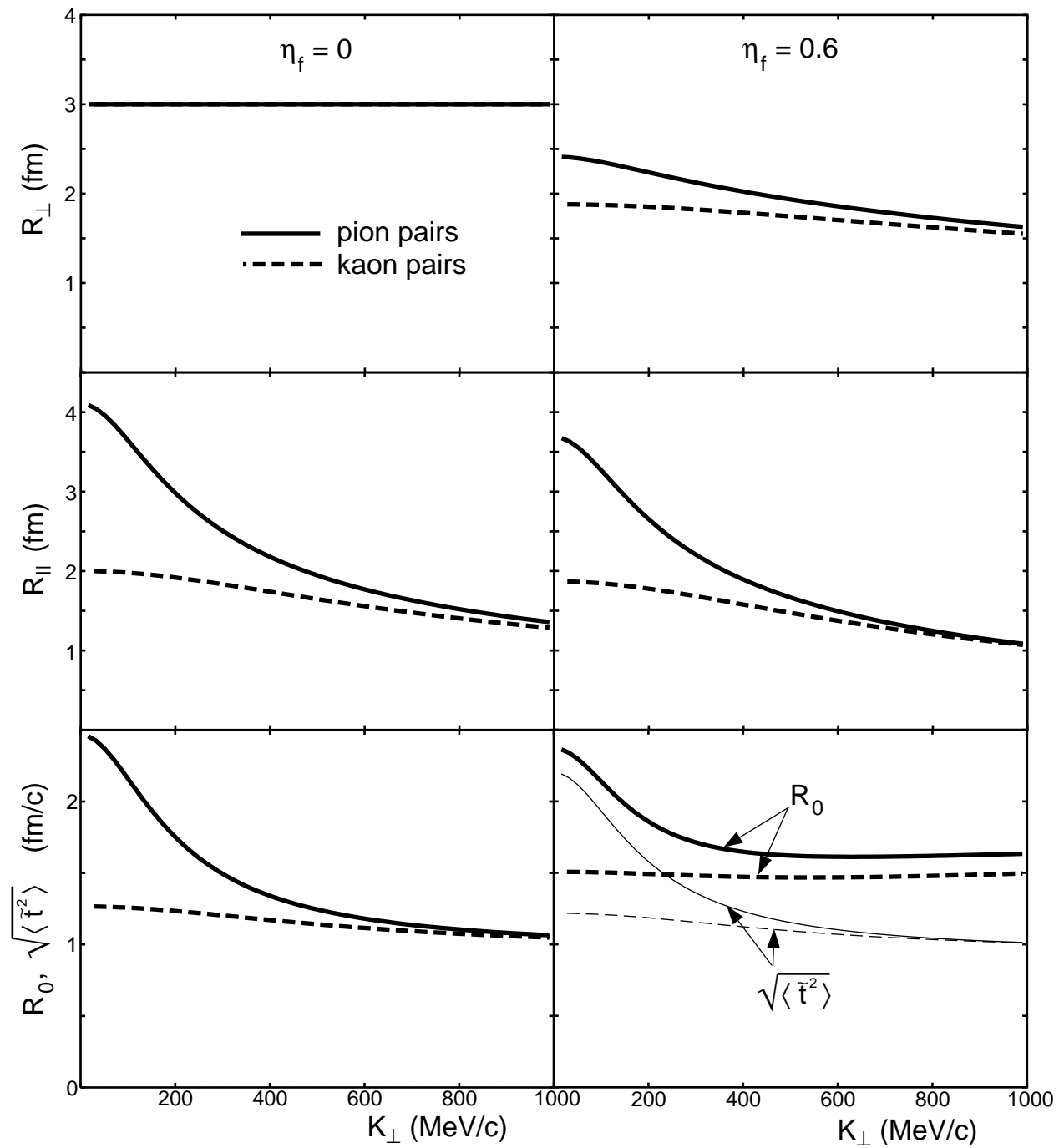


Fig.9

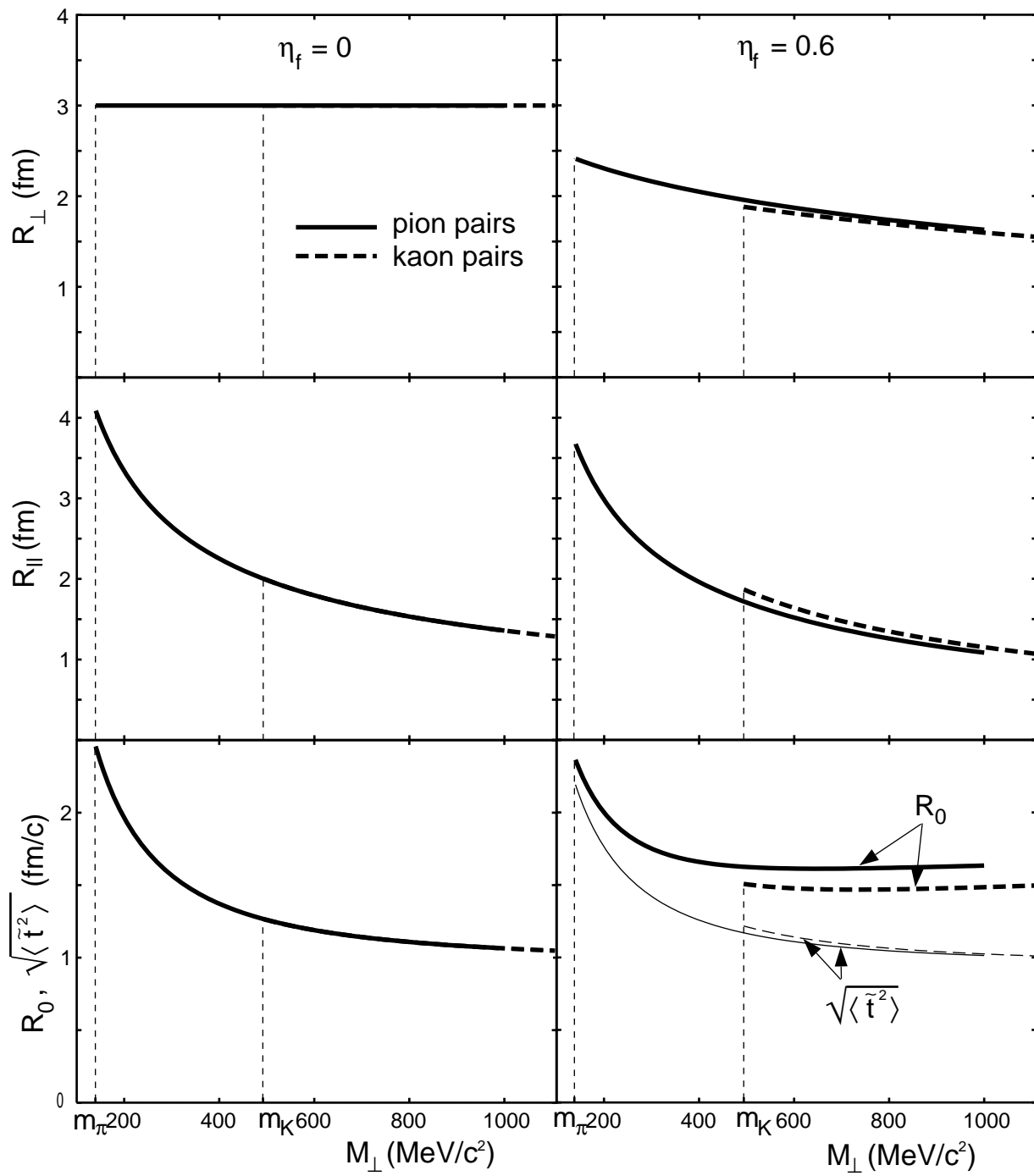


Fig.10



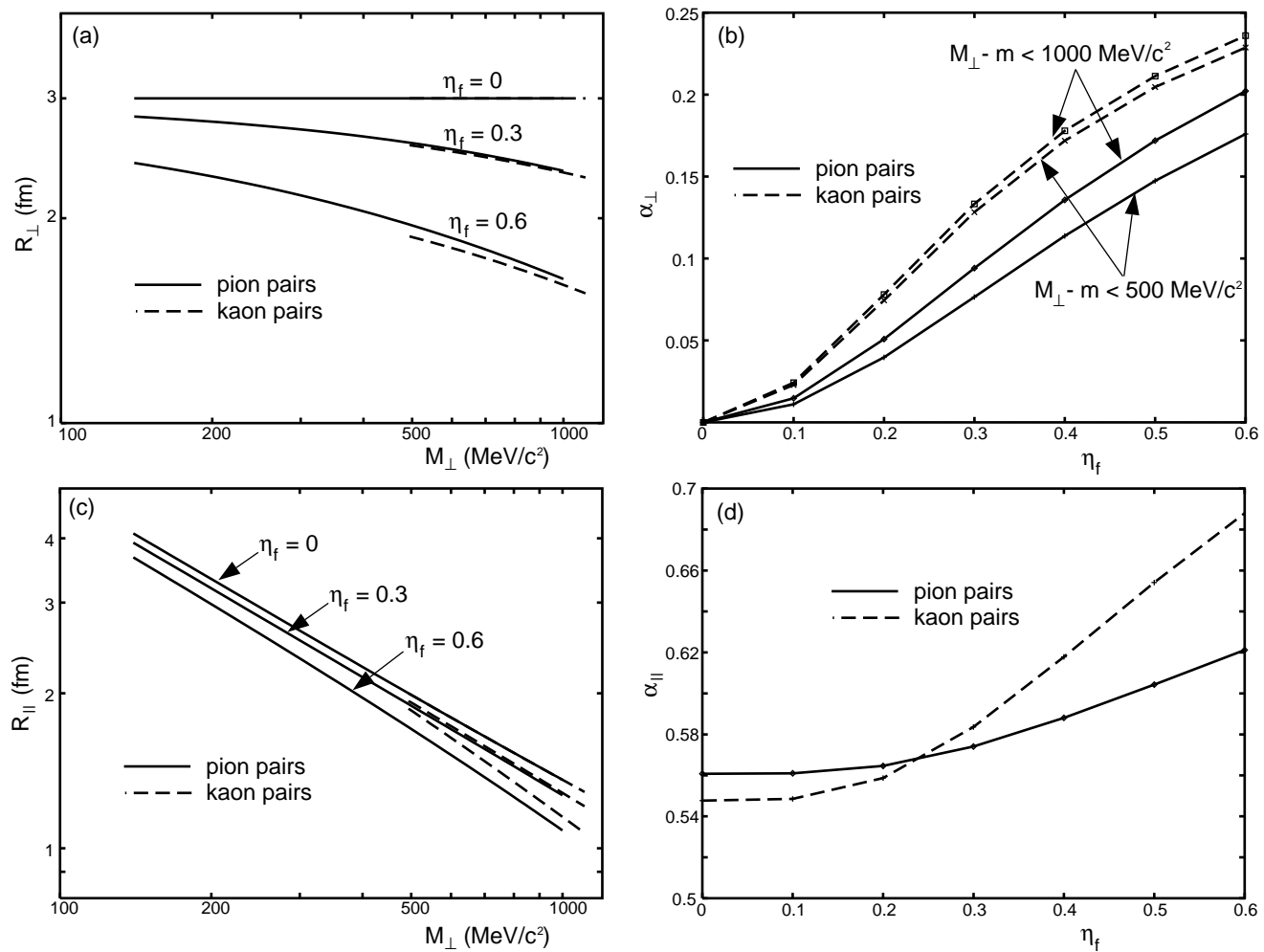


Fig.11